

Topology of the Interactions Pattern in Pharmaceutically Relevant Polymorphs of Methylxanthines (Caffeine, Theobromine, and Theophylline): Combined Experimental (^1H – ^{14}N Nuclear Quadrupole Double Resonance) and Computational (DFT and Hirshfeld-Based) Study

Jolanta Natalia Latosińska,* Magdalena Latosińska, and Grzegorz A. Olejniczak

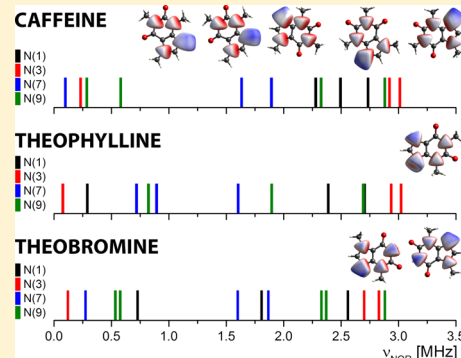
Faculty of Physics, Adam Mickiewicz University, Umultowska 85, 61-614 Poznań, Poland

Janez Seliger^{†,‡} and Veselko Žagar[†]

[†]“Jozef Stefan” Institute, Jamova 39, 1000 Ljubljana, Slovenia

[‡]Faculty of Mathematics and Physics, University of Ljubljana, Jadranska 19, 1000 Ljubljana, Slovenia

ABSTRACT: Three anhydrous methylxanthines: caffeine (1,3,7-trimethylxanthine; 1,3,7-trimethyl-1*H*-purine-2,6-(3*H*,7*H*)-dione) and its two metabolites theophylline (1,3-dimethylxanthine; 1,3-dimethyl-7*H*-purine-2,6-dione) and theobromine (3,7-dimethyl-xanthine; 3,7-dimethyl-7*H*-purine-2,6-dione), which reveal multifaceted therapeutic potential, have been studied experimentally in solid state by ^1H – ^{14}N NMR-NQR (nuclear magnetic resonance–nuclear quadrupole resonance) double resonance (NQDR). For each compound the complete NQR spectrum consisting of 12 lines was recorded. The multiplicity of NQR lines indicates the presence of a stable β form of anhydrous caffeine at 233 K and stable form II of anhydrous theobromine at 213 K. The assignment of signals detected in NQR experiment to particular nitrogen atoms was made on the basis of quantum chemistry calculations performed for monomer, cluster, and solid at the DFT/GGA/BLYP/DPD level. The shifts due to crystal packing interactions were evaluated, and the multiplets detected by NQR were assigned to N(9) in theobromine and N(1) and N(9) in caffeine. The ordering theobromine > theophylline > caffeine site and theophylline < theobromine < caffeine according to increasing electric field gradient (EFG) at the N(1) and N(7) sites, respectively, reflects the changes in biological activity profile of compounds from the methylxanthines series (different pharmacological effects). This difference is elucidated on the basis of the ability to form intra- and intermolecular interactions (hydrogen bonds and π ··· π stacking interactions). The introduction of methyl groups to xanthine restricts the ability of nitrogen atoms to participate in strong hydrogen bonds; as a result, the dominating effect shifts from hydrogen bond (theobromine) to π ··· π stacking (caffeine). Substantial differences in the intermolecular interactions in stable forms of methylxanthines differing in methylation (site or number) were analyzed within the Hirshfeld surface-based approach. The analysis of local environment of the nitrogen nucleus permitted drawing some conclusions on the nature of the interactions required for effective processes of recognition and binding of a given methylxanthine to A₁–A_{2A} receptor (target for caffeine in the brain). Although the interactions responsible for linking neighboring methylxanthines molecules in crystals and methylxanthines with targets in the human organism can differ significantly, the knowledge of the topology of interactions provides reliable preliminary information about the nature of this binding.



INTRODUCTION

The search for new drugs of natural origins belongs to one of the most dynamically developing branches of the pharmaceutical industry. The advantage of this approach is the fact that the influence of these compounds has long-term known effects on the human organism. Subtle differences in binding with targets are one of the most important factors, which have to be taken into account in the process of drug evaluation or development. For this reason, detailed structural investigation of natural products could be inspiring to improve solubility, search for

new biological targets, and discover new applications. In this paper, we report a study of three methylxanthines: caffeine (1,3,7-trimethylxanthine; 1,3,7-trimethyl-1*H*-purine-2,6-(3*H*,7*H*)-dione), theophylline (1,3-dimethylxanthine; 1,3-dimethyl-7*H*-purine-2,6-dione), and theobromine (xantheose; 3,7-dimethyl-xanthine; 3,7-dimethyl-7*H*-purine-2,6-dione); Figure 1. All these three purinic alkaloids occur naturally, in the

Received: July 16, 2014

Published: September 3, 2014



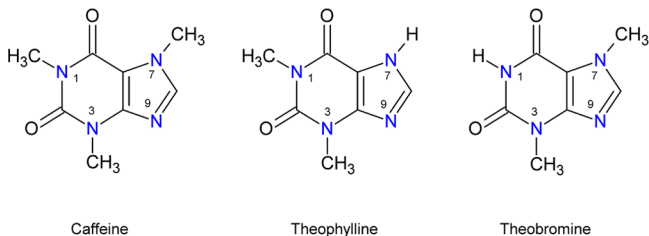


Figure 1. Chemical structures of methylxanthines with atom numbering.

leaves, seeds, or fruits of more than 60 plants. They were found in varying amounts in tea (*Camellia sinensis*¹ and *Ilex paraguaiensis*²) leaves, coffee (*Coffea Arabia*, *Coffea canephora var. Robusta*, *Coffea liberica*, and *Coffea dewevre*) beans,³ guaraná (*Paulinia guarana*) seeds,⁴ and cocoa (*Theobroma cacao*) nuts.⁵ It is believed that they make a part of the natural defense used by plants to poison herbivores, larvae of mealworms, mosquitos,⁶ and tobacco hornworms (i.e., they are natural insecticides) and to repel slugs and snails.⁷ They are also considered to be a part of a rewarding system—pharmacological manipulation of bees and other pollinator's behavior by associating floral scent with food while foraging (scent signals).^{8,9} Recently, the use of theophylline in the treatment of hyposmia (lost of smell sense) has been reported.¹⁰ All three methylxanthines belong to the pharmacological group of adenosine A-receptor (A₁, A₂, and A₃) antagonists¹¹ and act by the inhibition of cyclic GMP (guanosine monophosphate) and GABA_A (γ -aminobutyric acid)-receptors. A parent compound (caffeine) affects fundamental human processes such as sleep, arousal, cognition, learning, and memory and is able to stimulate central nervous system, as well as muscular, respiratory, and circular systems.^{12–15} It has the ability to reduce the physical, cellular, and molecular damages caused by a spinal cord injury (SCI), stroke (cerebral infarction), or neurodegenerative chronic diseases including diabetes II as well as Parkinson^{16–18} and Alzheimer's diseases^{19–21} the development of which it also inhibits. In addition, caffeine exhibits inhibitory activity against gallstones and cirrhosis of the liver and it is believed that it may reduce the risk of stroke.²² A broad spectrum of its action comes from the metabolites (12% of theobromine, vasodilator, diuretic, and heart stimulant,²³ 4% of theophylline, relaxing smooth muscles of the bronchi and effective in chronic obstructive pulmonary disease, asthma, and infant apnea, a drug with a long medical history which still used,²⁴ and 84% of paraxanthine, acting similarly to caffeine²⁵). Although all three compounds contain methyl groups, which may induce gene mutations²⁶ in mammals and man, the direct evidence *in vivo* of caffeine and theophylline effects is limited and they are classified as GRAS ("generally recognized as safe"). Their habitual consumption has been associated with a reduced risk of terminal diseases including liver, kidney, basal, and colorectal cancers.^{27–30} Recently, it has been discovered that they are able to decrease the mutagenic effect of UV (ultraviolet) radiation^{31–33} and some anticancer drugs.³⁴ Although theobromine is linked to mutations in eukaryotes, bacteria, and specifically cultured mammalian cells,^{35–37} its use as an anticancer agent has been patented.³⁸ This is in agreement with the observation that each anticancer drug can be carcinogenic.³⁹

Recently, caffeine and its derivatives have raised great attention mainly due to the possibility of designing dual-

target-directed drugs that simultaneously inhibit monoamine oxidase (MAO-B) and antagonize adenosine A_{2A} receptors (AA_{2A}R) in the brain.⁴⁰ Such compounds may offer unique activity of enhanced symptomatic relief and slowdown of Parkinson's and Alzheimer's diseases by protecting against further neurodegeneration.⁴¹

The differences in the spectra of activity of these compounds which do not operate in a synergistic manner⁴² can be explained on the molecular level. The xanthine core composed of two fused rings, a pyrimidinedione and imidazole, is common in the methylxanthines studied, the differences are limited to the number and site of substitution of methyl groups; Figure 1. Although these changes are limited to N(1) and N(7) nitrogen atoms they impose restrictions on the participation of the whole molecule in intermolecular interactions. Theobromine and theophylline are amphoteric thanks to the ability to accept protons at N(9) and to donate protons from N(7) in a case of theophylline and from N(1) in theobromine. The ability of N(9) to accept proton and the presence of proton migration channels (keto-enol tautomerism) makes these naturally basic compounds weakly acidic so able to form salts with acids and bases.⁴³ In contrast to theobromine and theophylline, caffeine has almost pure alkali nature. Due to the lack of the possibility of tautomerisation it is believed that it can form only a weak type of hydrogen bond using an N(9) atom as the only one possible acceptor. As follows from SAR (structure-activity relationship) studies⁴⁰ for the biological activity N(9) position is not important. Methyl groups substituted at N(1) and N(3) determine MAO-B inhibition, while at N(7) enhance both MAO-B activity and A_{2A} antagonism.⁴⁴ In general the ordering of methylxanthines according to the known pharmacological effect on the Central Nervous System (and also respiratory and skeletal muscle stimulation)

$$\text{Caffeine} > \text{Theophylline} > \text{Theobromine} \quad (1)$$

is different than that according to cardiac stimulation, coronary dilatation, smooth muscle relaxation, diuresis, and goitrogenic potential, i.e.

$$\text{Theophylline} > \text{Theobromine} > \text{Caffeine} \quad (2)$$

According to the literature the source of the difference between 1 and 2 is unclear.

Detailed analysis of the interaction pattern can deliver some beneficial clues for designing new inhibitors as dual-target-directed drugs with desired pharmacokinetic properties. Although the interactions responsible for linking the neighboring methylxanthines molecules in crystals and methylxanthines with targets in the human organism can differ significantly, the knowledge of the topology of crystal packing and shape of potential often provides reliable preliminary information about the nature of this binding.

The experimental technique which is able to describe very accurately the electric charge distribution in the neighborhood of the nitrogen atoms —N=, —NH, or —NCH₃ is ¹H-¹⁴N nuclear quadrupole double resonance (NQDR).⁴⁵ The components of the electric field gradient (EFG) tensor at the nucleus site describe the potential in the vicinity of the quadrupolar nucleus. The subtle differences in ¹⁴N NQR spectra allow analysis of the nature of the inter- and intramolecular interaction network from this local single nitrogen nucleus perspective. It gives some clues on the effect of methylation of nitrogen atoms on their binding abilities as well as the differences in solubility. In our previous studies, the

use of complementary methods local—experimental ^1H — ^{14}N NQDR—and global—theoretical DFT (density functional theory)—and Hirshfeld surfaces was found extremely helpful for clarifying the details of crystalline structure.^{46,47} We hope that this study will contribute to the explanation of implications of substitution on the formation of intermolecular bonding required for effective processes of recognition and binding caffeine and its derivatives with A_{2A} adenosine A₁-receptors.⁴⁸ These results of our present study can be used for prediction of the ability to form intermolecular interactions by caffeine-inspired compounds of great practical importance like potential therapeutic agents for treatment of asthma, cancer, diabetes, and Alzheimer's and Parkinson's diseases.

■ EXPERIMENTAL SECTION

The polycrystalline samples of anhydrous caffeine ($\text{C}_8\text{H}_{10}\text{N}_4\text{O}_2$), theobromine ($\text{C}_7\text{H}_8\text{N}_4\text{O}_2$), and theophylline ($\text{C}_7\text{H}_8\text{N}_4\text{O}_2$) were purchased from Sigma-Aldrich and used without further recrystallization or any additional purification. The purity of samples was confirmed to be above 98%. Anhydrous theophylline and caffeine were identified as polymorphic form II and β and used as received. Each ^1H — ^{14}N NQDR measurement was performed on a sample of about 0.5 g. The powdered samples were degassed and sealed in glass ampules. Three different double resonance techniques based on magnetic field cycling were used to search for ^{14}N NQR frequencies. The first method was the ^1H — ^{14}N cross relaxation spectroscopy,⁴⁹ then the solid-effect technique,⁵⁰ and finally the two-frequency irradiation technique.⁵¹ In the level crossing⁵² and solid-effect⁵³ techniques during the relaxation period a strong rf magnetic field of a frequency ν is applied. A decrease in the proton NMR signal is observed when ν is equal to the ^{14}N NQR frequency ν_Q (level crossing) and when ν is equal to $\nu_Q \pm \nu_H$ (solid effect). Here $\nu_H = \gamma_H B / 2\pi$ is the proton Larmor frequency in the low magnetic field B . After a scan at the frequency ν , the ν -dependence of the proton NMR signal shows that the level crossing reaches minima (dips) at $\nu = \nu_Q$ ($Q = +, -, 0$) and the solid effect at $\nu = \nu_Q \pm \nu_H$.

In the NQDR technique with the multiple frequency sweeps of rf magnetic field and two-frequency irradiation^{54,55} at first the multiple frequency sweeps of rf magnetic field are applied during the relaxation period. The sweep range is chosen so that it covers the higher ^{14}N NQR frequencies ν_+ and ν_- . Always when during the sweep the frequency of the rf magnetic field reaches the ^{14}N NQR frequency ν_Q ($Q = +, -$), the population of the two ^{14}N nuclear quadrupole energy levels separated in frequency by ν_Q changes. A scan is performed by the low magnetic field B in steps of 0.25 mT. When the proton Larmor frequency ν_H in the low magnetic field B matches the lowest ^{14}N NQR frequency ν_0 , the multiple frequency sweeps produce a relaxation of the proton magnetization toward zero which is observed as a decrease in the proton NMR signal at the end of the magnetic field cycle. In the ν_H dependence of the proton NMR signal, a dip is observed at $\nu_H = \gamma_H B / 2\pi = \nu_0$.

In the second step of the experiment, the low magnetic field B is fixed at this dip and the scan is performed by one of the frequency limits (say the upper limit) of the frequency sweeps. When the upper frequency limit becomes lower than ν_+ , the frequency sweeps cover only ν_- and they do not produce a relaxation of the proton magnetization toward zero. So when the upper sweep frequency limit passes ν_+ from above, the proton NMR signal increases. For a similar reason the proton

NMR signal increases also when the lower sweep frequency limit passes ν_- from below and the upper sweep frequency limit is fixed above ν_+ . In such a way ν_+ , ν_- , and ν_0 are determined to an accuracy of approximately 10 kHz. Moreover, with this technique it is possible to separate in the complex ^{14}N NQR spectrum the triplets ν_+ , ν_- , and ν_0 corresponding to various inequivalent nitrogen positions in the crystal. In the final step of the experiment, during the relaxation period, the condition $\nu_H = \nu_0$ is satisfied and two rf magnetic fields of frequencies ν_1 and ν_2 are applied. When $\nu_1 = \nu_-$ and $\nu_2 = \nu_+$, we observe a relaxation of the proton magnetization toward zero. Performing the scans at the frequencies ν_1 and ν_2 , the accuracy of determination of the ^{14}N NQR frequencies is increased to about 5 kHz or better, depending mainly on the magnetic field broadening of the ^{14}N NQR lines during the relaxation period. The application of all the three double resonance techniques has ensured unambiguous determination of the triplets (ν_+ , ν_- , and ν_0) of the ^{14}N NQR frequencies arising from various chemically/physically nonequivalent positions of nitrogen atoms in molecule/crystal.

■ QUANTUM CHEMISTRY CALCULATIONS

Quantum chemical calculations were carried out within the GAUSSIAN09⁵⁶ and DMOL^{357,58} codes run on the CRAY supercomputer at the Poznan Supercomputer and Network Centre (PCSS) in Poznan, Poland. The calculations were performed within the Density Functional Theory (DFT) with exchange-correlation hybrid functional: B3LYP (three-parameter exchange functional of Becke B3⁵⁹ combined with the Lee-Yang-Parr correlation functional LYP⁶⁰) using the extended basis sets with polarization and diffuse functions 6-311+ +G(d,p) and BLYP (functional of Becke B88⁵⁹ combined with the Lee-Yang-Parr correlation functional LYP⁶⁰) with numerical radial functions basis—double- ζ basis set. The calculations were carried out under the assumption of the monomer, cluster, or solid (periodic boundary conditions) using crystallographic geometry. The principal components of second rank symmetric electric field gradient (EFG) tensor, $q_{ii} = \partial^2 V(r) / \partial x_i^2$ ($i = x, y$, and z ; $V(r) = (1/4\pi\epsilon_0) \int_V [\rho(r') / |r - r'|] dV$ —external electrostatic potential, $\rho(r)$ is the electron density, r_i is the projection of r vector onto x , y , and z axes) satisfying the relation $|q_{xx}| \leq |q_{yy}| \leq |q_{zz}|$, were evaluated as eigenvalues of symmetric matrix using Lanczos diagonalization method. ^{14}N NQR frequencies usually named as $\nu_+ > \nu_- \geq \nu_0$ were calculated from

$$\begin{aligned} \nu_+ &= \left| \frac{e^2 q Q}{4h} \right| (3 + \eta) \\ \nu_- &= \left| \frac{e^2 q Q}{4h} \right| (3 - \eta) \\ \nu_0 &= \nu_+ - \nu_- = \left| \frac{e^2 q Q}{2h} \right| \eta \end{aligned} \quad (3)$$

where $e^2 Qq/h = e^2 Qq_{zz}/h$ is the nuclear quadrupole coupling constant and $\eta = (q_{xx} - q_{yy})/q_{zz}$ is the asymmetry parameter. The nuclear quadrupole moment for ^{14}N equal to 2.044 fm² (ref 61) was assumed. The quadrupole coupling constant $e^2 q Q/h$ and the asymmetry parameter η for ^{14}N nucleus are related to these frequencies by the formulas:

Table 1. Experimental ^1H – ^{14}N NQDR Parameters for Caffeine, Theophylline, and Theobromine

compound	site	^1H – ^{14}N NQDR					T [K]
		$ e^2 Qq/h $ [MHz]	η	ν_+ [MHz]	ν_- [MHz]	ν_0 [MHz]	
caffeine	>N(1)CH ₃ ^a	3.520	0.136	2.760	2.520	0.240	233
	>N(3)CH ₃	3.967	0.045	3.020	2.930	0.090	
	>N(7)CH ₃	2.340	0.222	1.885	1.625	0.260	
	–N(9)= ^b	3.437	0.323	2.855	2.300	0.555	
theophylline	>N(1)CH ₃	3.429	0.184	2.730	2.414	0.316	213
	>N(3)CH ₃	3.984	0.043	3.031	2.945	0.086	
	>N(7)H	1.653	0.859	1.595	0.885	0.710	
	–N(9)=	3.025	0.527	2.667	1.870	0.797	
theobromine	>N(1)H ^c	2.942	0.511	2.582	1.831	0.751	295
	>N(3)CH ₃ ^c	3.697	0.070	2.837	2.708	0.129	
	>N(7)CH ₃ ^c	2.301	0.232	1.859	1.592	0.267	
	–N(9)= ^d	3.470	0.295	2.858	2.347	0.511	
		3.442	0.321	2.858	2.305	0.553	

^aBroad unresolved lines, five noneq molecules in unit cell. ^bBroad unresolved lines. ^cLines not split within exp resolution. ^dTwo nonequivalent molecules in a unit cell.

$$\left| \frac{e^2 qQ}{h} \right| = \frac{2}{3}(\nu_+ + \nu_-)$$

$$\eta = \frac{3(\nu_+ - \nu_-)}{\nu_+ + \nu_-} \quad (4)$$

while the principal values of the nuclear quadrupole coupling q_{ii} tensor is related by the following equations:

$$q_{zz} = \frac{e^2 qQ}{h}$$

$$q_{yy} = -\frac{e^2 qQ}{2h}(1 + \eta) = -\frac{q_{zz}}{2}(1 + \eta)$$

$$q_{xx} = -\frac{e^2 qQ}{2h}(1 - \eta) = -\frac{q_{zz}}{2}(1 - \eta) \quad (5)$$

■ HIRSHFELD SURFACE

Theoretical analysis of intermolecular interactions pattern was performed within the Hirshfeld surfaces approach.⁶² The Hirshfeld surface^{62,63} in a crystal is a region where the *promolecule* (electron density from spherical atoms of the molecule) dominates over the *procrystal* (electron density from spherical atoms of the crystal). Numerically this condition is described with the use of the molecular weight-function $w(r)$:

$$w(r) = \frac{\sum_{A \in \text{molecule}} \rho_A(r)}{\sum_{A \in \text{crystal}} \rho_A(r)} \geq 0.5 \quad (6)$$

where summation of spherically averaged atomic electron density centered on nucleus A, $\rho_A(r)$, runs over the atoms belonging to the molecule (numerator) and to the crystal (denominator), respectively. Electrostatic potential mapped on the Hirshfeld surface shows the positions of close intermolecular contacts, while the shape index and curvedness exhibit $\pi \cdots \pi$ stacking interactions. Decomposition of the Hirshfeld surface into a 2D “molecular fingerprint” map provides a quantitative characteristics, the distribution of interactions of the molecule with its environment.

■ RESULTS AND DISCUSSION

The experimental NQR frequencies obtained for caffeine, theobromine and theophylline and NQR parameters derived from them using eqs 3 and 4 are collected in Table 1. From among these compounds, only in the spectrum of theophylline are there lines that are not broadened. The NQR spectra of caffeine and theobromine are characterized by both additional signals and broadened NQR signals unlike the “clean” spectrum of the theophylline. The character of both spectra suggests the presence of unequivalent molecules per unit cell; the broadening suggests also some structural disorder. For a more detail analysis the appropriate assignment of NQR frequencies to the particular nitrogen sites was required. Some clues come directly from a comparison of NQR parameters with those obtained earlier for benzimidazoles,⁶⁴ thioureas,⁴⁵ other xanthines,⁶⁵ but it was not enough to make a reliable assignment. Therefore, the final assignment, shown in Figure 2 and Table 1, was made with the help of quantum chemistry calculations. For many compounds, a reliable reproduction of the components of EFG tensor can be obtained using the clustering technique.⁶⁶ For methylxanthines, the differences between particular methylated nitrogen sites, >NCH₃, are subtle and taking into account distant effects can be vital. Thus, the NQR parameters were calculated using two different techniques: clustering/B3LYP/6-311++G** and solid simulation GGA/BLYP/DPD (periodic boundary conditions). The X-ray^{67–69} geometries, Table 2, were assumed. The results are collected in Table 3 and shown in Figure 3. The reproduction of NQR parameters, irrespective of the level of theory and kind of model (molecule, cluster or crystal) is charged with a relatively small error (correlation coefficients 0.969, 0.974, and 0.982 for molecule, cluster or crystal, respectively), Figure 3. The results obtained at the B3LYP level of theory assuming the cluster formation, are nearly as good (less overestimated) as those obtained at BLYP level assuming the solid state. Both are significantly better than those obtained assuming the monomer formation. The degree of agreement between the calculated NQR parameters and the experimentally determined ones is the criterion for the goodness of an approximate ground state wave function and informs about the quality of approximation of the electron density distribution, calculated only on the basis of the assumed crystallographic structure, to the real

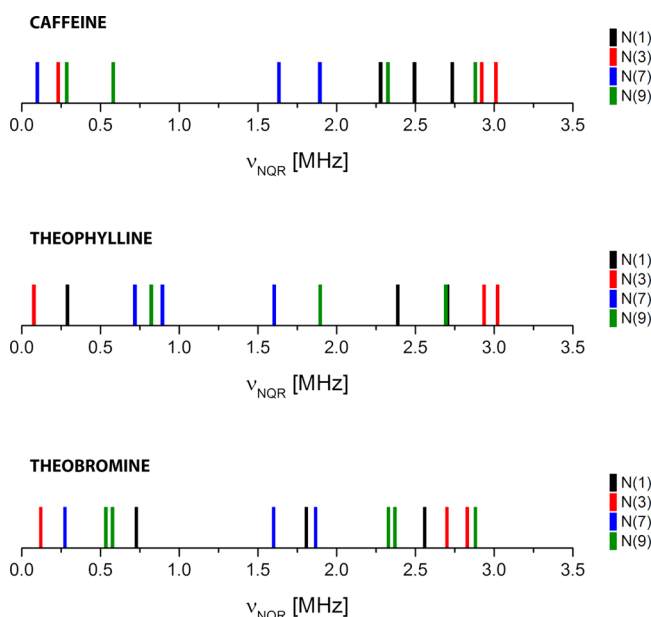


Figure 2. Positions and assignment of signals detected in NQR experiment to particular nitrogen atoms in caffeine, theophylline, and theobromine.

distribution in the crystals of methylxanthines. This point is highly significant from the viewpoint of reliability of further analysis of interactions. Irrespective of the quantitative result (assumed model or level of the theory), the qualitative result, that is the assignment of NQR signals to particular nitrogen sites, is the same, Tables 1 and 3. The validity of this assignment was verified by deformation density calculations at GGA/BLYP/DPD level. Deformation density maps, which reveal the difference between the total electron density and the electron density of “neutral spherical unperturbed atoms” superimposed at the same nuclear positions, for the monomer and cluster of each compound studied, are shown in Figure 4. The high symmetry surrounding of N(9) and low symmetry at N(3), Table 1, are well reflected by high and low values of the asymmetry parameter of EFG tensor, even for isolated molecules, Table 3. This indicates that the electrostatic charge distribution within a single molecule and, in the first approximation, its nearest neighbors determine the EFG tensor in methylxanthines, while the crystalline network only modulates it.

Caffeine. Caffeine occurs as two solid polymorphs, stable (β), which is a final product of dehydration process, and metastable (α) which appears upon heating at 418–426 K^{70,71}

shortly before melting point at 509 K and reverts into β form at room temperature. Form β of anhydrous caffeine, stable at RT, is the most commonly used in formulations of solid dosage forms. After many attempts to solve the crystal structure of anhydrate caffeine, Stowasser and Lehmann⁶⁷ suggested that β form of anhydrous caffeine crystallizes with five crystallographically inequivalent molecules in a monoclinic C-centered $C2/c$ unit cell with dimensions of $a = 43.0390$, $b = 15.0676$, and $c = 6.95314$ Å and β angle of 99.027°, Table 2, while Derolle et al.⁷² indicated a highly disordered structure of the metastable phase α , a rhombohedral $R3c$ unit cell with $Z = 6$ and $a = 14.9372$, $b = 14.9372$, $c = 6.8980$ Å, and a γ angle of 120°. Both structures β and α , have been recently reinvestigated at 100 and 125 K, respectively, by Enright et al.⁷³ The character of the $^1\text{H}-^{14}\text{N}$ NQR spectra of caffeine recorded at 233 K, confirms the presence of form β in the studied sample. For the nitrogen site N(1) there was a clear indication of a multiplet consisting of five lines, for N(9), the lines were broadened, while for the other two nitrogen sites the experimental resolution was too small and the lines could not be well resolved, Table 1 and Figure 2. A comparison of NQR parameters at the corresponding nitrogen sites in inequivalent molecules calculated for each molecule taken from the caffeine crystal (monomer) reveals negligible differences, Table 3. These differences are a bit more pronounced in the solid state (the largest in e^2Qq_{zz}/h at N(3) and in η at N(7)); Table 3, Figure 3. The discrepancy between experiment and calculations for N(9) site suggests that the broadening of NQR line assigned to this site is a dynamical effect. This conclusion is in good agreement with our previous observation made for Cladribine.⁴⁷

Comparison of the deformation density maps, Figure 4, and NQR parameters obtained under assumption of monomer and solid state formation, Figure 3, Table 3, suggests that the intermolecular interactions in caffeine are weak and rather not directional. The intermolecular interaction pattern in the crystal (hydrogen bonds, hydrogen–hydrogen contacts in methyl groups and $\pi-\pi$ stacking) can be readily identifiable by means of molecular Hirshfeld surface. The Hirshfeld surface with the normalized contact distance d_{norm} for the vicinities of each nitrogen and the whole caffeine molecule in each inequivalent caffeine molecule are shown in Figure 5a. Figure 5b and c shows the Hirshfeld surface with the mapped curvedness and shape index for all five inequivalent molecules. More details on the interactions pattern obtained from analysis of 2D fingerprint plots is quantitatively summarized in Table 4. At the first sight, the volume and shape of surfaces are similar but the comparison of their volumes, surfaces, globularity, and

Table 2. Comparison of Structural Data for a Set of Methylxanthines Caffeine, Theophylline, and Theobromine (Pharmaceutically Relevant Polymorphic Forms)

	caffeine (stable form β) ^{73,67}		theophylline (stable form II) ^{68,85}		theobromine (stable form) ⁶⁹
R factor [%]	5.84 ⁷³	4.33 ⁶⁷	4.16 ^{85b}	5.3 ⁶⁸	N/A ^{85a}
T [K]	100	RT	120	293	RT
space group	$C2/c$	$C2/c$	$Pna2_1$	$Pna2_1$	$P2_1/c$
α [°]	90	90	90	90	90
β [°]	97.825(4)	99.0274(22)	90	90	91.75(3)
γ [°]	90	90	90	90	90
a [Å]	42.521(9)	43.0390(17)	24.330(1)	24.612 (2)	24.628(4)
b [Å]	14.948(3)	15.06758(64)	3.7707(2)	3.8302 (4)	3.833(2)
c [Å]	6.7923(14)	6.95314(14)	8.4850(5)	8.5010 (5)	8.501(5)

Table 3. ^{14}N NQR Parameters Calculated at the GGA/BLYP/DND Level for Caffeine, Theophylline, and Theobromine (Monomer, Cluster, and Solid)

Compound	Molecule*	Site	monomer						cluster						PBC/solid					
			$ \epsilon^2\text{Qqh}^{-1} $ [MHz]	η	v_+ [MHz]	v_- [MHz]	v_0 [MHz]		$ \epsilon^2\text{Qqh}^{-1} $ [MHz]	η	v_+ [MHz]	v_- [MHz]	v_0 [MHz]	$ \epsilon^2\text{Qqh}^{-1} $ [MHz]	η	v_+ [MHz]	v_- [MHz]	v_0 [MHz]		
CAFFEINE	K1		4.233	0.106	3.287	3.063	0.225	4.257	0.087	3.285	3.100	0.185	4.032	0.166	3.191	2.857	0.334			
	K2		4.232	0.107	3.287	3.061	0.226	4.219	0.122	3.293	3.036	0.257	4.185	0.113	3.257	3.020	0.237			
	N(1)		4.229	0.106	3.284	3.059	0.225	4.215	0.112	3.279	3.043	0.236	4.117	0.146	3.238	2.938	0.300			
	K4		4.230	0.107	3.286	3.059	0.227	4.222	0.109	3.282	3.051	0.230	4.249	0.091	3.283	3.090	0.193			
	K5		4.231	0.107	3.286	3.061	0.225	4.238	0.105	3.290	3.067	0.222	4.058	0.170	3.216	2.871	0.345			
	avg. K1-5**		4.231	0.107	3.286	3.061	0.226	4.230	0.107	3.286	3.059	0.226	4.128	0.137	3.237	2.955	0.282			
	K1		4.650	0.023	3.515	3.460	0.054	4.530	0.036	3.438	3.357	0.082	4.503	0.049	3.433	3.322	0.111			
	K2		4.650	0.024	3.515	3.460	0.055	4.657	0.012	3.507	3.479	0.028	4.399	0.087	3.395	3.204	0.191			
	N(3)		4.648	0.024	3.513	3.459	0.055	4.625	0.016	3.487	3.450	0.037	4.428	0.038	3.363	3.278	0.084			
	K4		4.648	0.024	3.514	3.459	0.055	4.474	0.071	3.435	3.276	0.159	4.387	0.075	3.373	3.208	0.165			
	K5		4.648	0.023	3.513	3.459	0.054	4.525	0.024	3.421	3.367	0.054	4.634	0.024	3.504	3.447	0.056			
	avg. K1-5**		4.649	0.024	3.514	3.459	0.055	4.562	0.032	3.457	3.386	0.072	4.470	0.055	3.414	3.292	0.121			
THEOPHYLLINE	K1		3.266	0.180	2.597	2.303	0.294	3.254	0.186	2.592	2.289	0.303	3.076	0.164	2.432	2.181	0.251			
	K2		3.265	0.180	2.596	2.302	0.293	3.077	0.166	2.435	2.180	0.255	3.145	0.175	2.496	2.221	0.275			
	N(7)		3.267	0.179	2.596	2.304	0.292	3.136	0.176	2.490	2.214	0.276	3.009	0.217	2.419	2.094	0.326			
	K4		3.267	0.180	2.597	2.303	0.294	3.273	0.176	2.599	2.311	0.288	3.126	0.196	2.498	2.191	0.307			
	K5		3.267	0.181	2.598	2.303	0.295	3.118	0.191	2.487	2.190	0.298	3.010	0.165	2.381	2.134	0.248			
	avg. K1-5**		3.266	0.180	2.597	2.303	0.294	3.172	0.179	2.521	2.237	0.284	3.073	0.183	2.445	2.164	0.281			
	K1		3.979	0.351	3.333	2.635	0.698	3.992	0.348	3.341	2.647	0.695	3.817	0.402	3.247	2.479	0.768			
	K2		3.977	0.351	3.332	2.633	0.698	3.899	0.375	3.290	2.559	0.731	3.831	0.394	3.250	2.495	0.755			
	N(9)		3.978	0.351	3.333	2.634	0.698	3.899	0.383	3.298	2.551	0.747	3.906	0.384	3.305	2.555	0.750			
	K5		3.978	0.351	3.332	2.634	0.698	3.917	0.370	3.300	2.575	0.725	3.815	0.422	3.263	2.459	0.805			
	avg. K1-5**		3.978	0.351	3.333	2.634	0.698	3.933	0.366	3.310	2.589	0.721	3.830	0.402	3.257	2.488	0.769			
THEOBROMINE	TP1	N(1)	4.307	0.131	3.371	3.090	0.281	4.125	0.174	3.273	2.914	0.359	4.045	0.188	3.224	2.844	0.380			
	TP1	N(3)	4.756	0.057	3.634	3.499	0.135	4.757	0.066	3.646	3.490	0.157	4.611	0.089	3.562	3.355	0.207			
	TP1	N(7)	3.063	0.236	2.478	2.117	0.361	3.028	0.258	2.467	2.076	0.391	2.403	0.772	2.266	1.338	0.927			
	TP1	N(9)	4.270	0.317	3.540	2.864	0.676	3.763	0.492	3.285	2.359	0.926	3.725	0.513	3.271	2.316	0.956			
	TB1		3.901	0.408	3.323	2.528	0.795	3.477	0.711	3.226	1.990	1.236	3.470	0.694	3.205	2.001	1.204			
	TB2		3.948	0.345	3.302	2.620	0.682	3.488	0.661	3.193	2.040	1.153	3.457	0.651	3.155	2.031	1.125			
	avg. TB1-2**		3.925	0.377	3.313	2.574	0.738	3.482	0.686	3.209	2.015	1.194	3.463	0.673	3.18	2.016	1.165			
	TB1		4.684	0.034	3.552	3.474	0.079	4.488	0.041	3.412	3.320	0.092	4.401	0.069	3.377	3.225	0.152			
	TB2	N(3)	4.659	0.049	3.551	3.437	0.114	4.465	0.056	3.412	3.287	0.125	4.417	0.066	3.386	3.240	0.146			
	avg. TB1-2**		4.671	0.041	3.551	3.455	0.096	4.476	0.048	3.412	3.304	0.108	4.409	0.067	3.3815	3.233	0.149			
THEOBROMINE	TB1		3.269	0.183	2.601	2.302	0.299	3.119	0.191	2.488	2.191	0.298	3.120	0.167	2.470	2.210	0.261			
	TB2	N(7)	3.299	0.171	2.615	2.333	0.282	3.139	0.166	2.484	2.224	0.260	3.061	0.144	2.406	2.186	0.220			
	avg. TB1-2**		3.284	0.177	2.608	2.318	0.291	3.129	0.179	2.486	2.208	0.279	3.091	0.156	2.438	2.198	0.241			
	TB1		3.789	0.415	3.235	2.448	0.787	3.674	0.448	3.167	2.344	0.823	3.563	0.497	3.115	2.229	0.885			
	TB2	N(9)	3.834	0.391	3.250	2.501	0.749	3.711	0.425	3.178	2.389	0.788	3.659	0.441	3.147	2.341	0.806			
	avg. TB1-2**		3.812	0.403	3.243	2.475	0.768	3.693	0.436	3.173	2.366	0.806	3.611	0.469	3.131	2.285	0.846			

*Inequivalent molecules. **Averaged values.

asphericity reveals notable differences, Table 4. The largest differences appear in the contacts (predominantly weak hydrogen bonds) in which the most electronegative atom, oxygen, participates. The hydrogen bonds C—H···X (X = O, N) of 2.787–3.341 Å linking protons from methyl groups are visualized as red areas in the Hirshfeld surface, Figure 5. Although their strength differs in the set of inequivalent molecules, this effect is poorly visible in this surface. In the 2D molecular fingerprint d_e/d_i plot these interactions are represented by the characteristic “wings” (two spikes top left and bottom right; reciprocal interactions included), Figure 6a and b. The wings at the top left, $d_i < d_e$, can be assigned to the surface around the donor (C—H bond), whereas those at the bottom right, $d_e > d_i$, correspond to the surface around the acceptor (O or N). Two sets of wings describing C—H···X (X = O, N) were poorly resolved thus they were extracted from the global 2D fingerprint plot, Figure 6a. The presence of many interactions differing slightly in length and strength results in wide spikes. The area corresponding to the contacts O···H/H···O and N···H/H···N takes from 20.9 to 24% and from 8.6 to 12.4% of the total Hirshfeld surface, respectively, Table 4. The whole 2D fingerprint plot for caffeine, especially in the central part, Figure 6a, is dominated by the presence of many H···H interactions (protons from methyl groups), which takes nearly 50% of the total Hirshfeld surface. These interactions are manifested as only one but highly broadened spike, indicating

the presence of many slightly differing in length and strength H···H interactions. Hirshfeld surfaces are also useful for identification of associates. The curvedness and shape index, which are sensitive to very subtle changes in the surface shape, particularly in the regions where the curvedness is very low, are shown in Figure 5b and c. The adjacent red and blue triangles varying slightly in size and shape from molecule to molecule clearly indicate that the crystal structure exhibits strong $\pi\cdots\pi$ stacking interactions between pairs of inequivalent molecules of about 3.473, 3.39, 3.355, 3.269, and 3.425 Å and -66.3, -69.7, -71.2, -68.6, and -71.5 kJ/mol. Energetically, the $\pi\cdots\pi$ stacking are the dominant motif in β form of crystalline structure. The analysis of local Hirshfeld for each nitrogen site separately reveals some additional details, Table 5, Figure 7a–f. Two-dimensional fingerprints for N(9) differ qualitatively and quantitatively from those for N(1), N(3), and N(7), Figure 7c–f and Table 5. Two wings for N(9), long and sharp at the top are assigned to the surface around the (N—C bonds), while small and wide at the bottom correspond to the surface around the (—N=), but only one for N(1), N(3), and N(7)—assigned to the surface around the N—C bonds—indicates different symmetry of the nitrogen vicinity and participation of N(9) in a weak bond, Figure 7. The limitation to spherically averaged atomic electron density does not allow the use of Hirshfeld surface or 2D fingerprints to differentiate subtle differences between methyl groups, Table 5, clearly

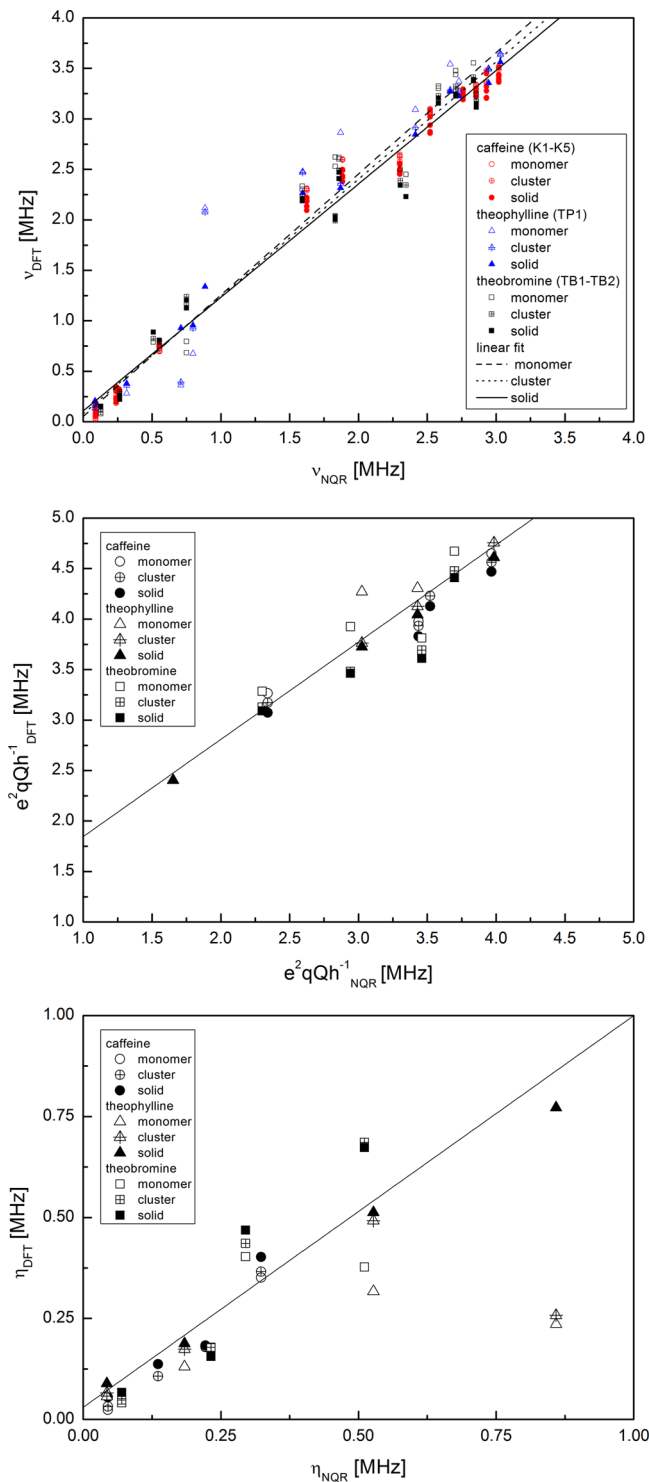


Figure 3. Correlation between experimental and calculated NQR parameters (a) frequencies (the scattering due to the presence of inequivalent molecules is indicated), (b) quadrupole coupling constants (the values averaged over all inequivalent molecules in the unit cell), and (c) asymmetry parameters (the values averaged over all inequivalent molecules in the unit cell), for all compounds studied.

visible on the deformation density map, Figure 4 a and in experiment, Table 1. The comparison of the shape of 2D fingerprint plot for each corresponding nitrogen site in all five inequivalent molecules reveals small differences, Table 4, Figure 6b, which is in good agreement with experiment. Much smaller

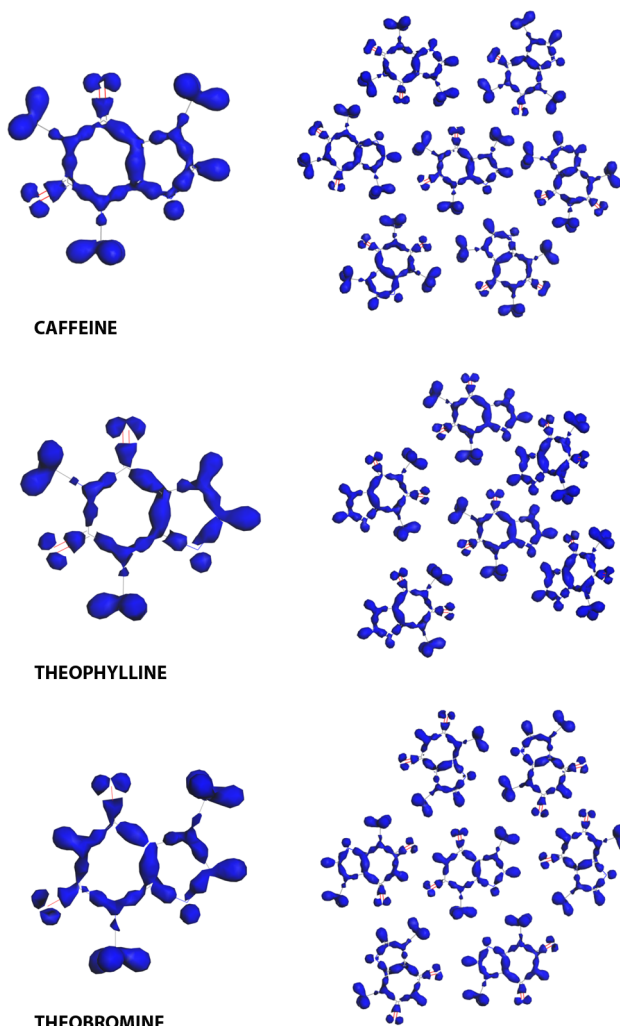


Figure 4. Deformation density maps (the difference between the total electron density and the electron density of “neutral spherical unperturbed atoms” superimposed at the same nuclear positions), for each compound studied (iso surface at 0.2 au).

than implied from X-ray data NQR frequencies, resulting in the lack of clear multiplicity in NQR spectra suggest the dynamical averaging. This conclusion well supports the hypothesis that β form is dynamically disordered.^{74,75}

Theophylline. Anhydrous theophylline is formed upon dehydration of monohydrated form by different methods, using the effect of solid-state transition, dehydration, and evaporation or vacuum drying of monohydrate.^{76,77} The question of anhydrous theophylline polymorphism has been widely discussed since 1943.⁷⁸ The existence of the high temperature form I has been reported by Doser⁷⁸ and later confirmed,^{79–81,68} forms II, III, and IV have been reported by Kahmar⁸² and Suzuki et al.,⁸¹ Matsuo and Matsuoka,⁷⁶ and Seton et al.,^{83,84} respectively. Crystal forms II and IV are stable, orthorhombic, and monoclinic, respectively. Form I is reported to be the stable at higher temperatures, but the phase transition of this form to form II (at 493 K) is very slow. Form III is highly metastable and rapidly converts to form II in solid state or in organic solvents. Form II of anhydrous theophylline, stable at RT, is the most commonly used in formulations of solid dosage forms.

Theophylline crystallizes in this form in $Pna2_1$ with cell unit dimensions varying from $a = 24.612$, $b = 3.8302$, and $c = 8.5010$

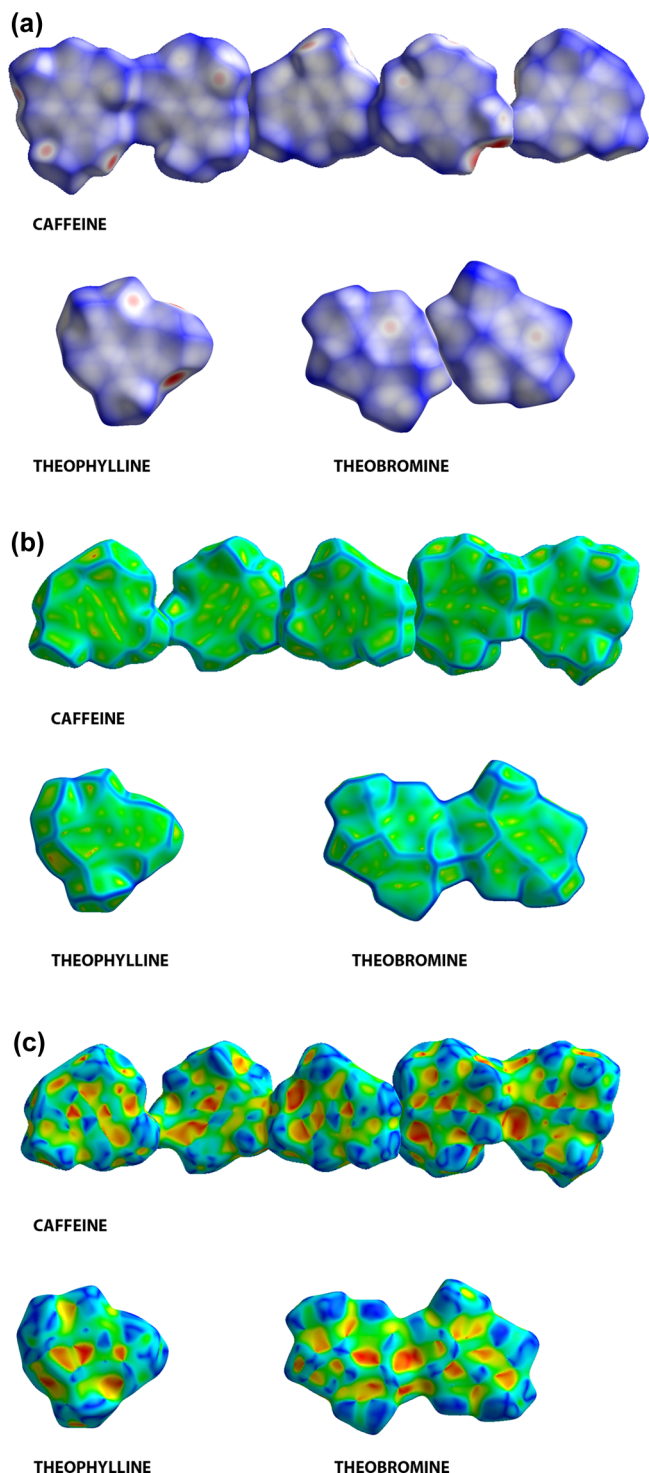


Figure 5. 3D Hirshfeld surface with the normalized contact distance d_{norm} for caffeine, theophylline, and theobromine. (b) 3D Hirshfeld surface with the mapped curvedness for caffeine, theophylline, and theobromine. (c) 3D Hirshfeld surface with the mapped shape index for caffeine, theophylline, and theobromine.

\AA to $a = 24.330$, $b = 3.7701$, and $c = 8.4850 \text{ \AA}$ in 100 K and RT, respectively, Table 2.^{68,85} The main motifs in this form are NH \cdots N hydrogen bonds, (involving the best donor (the NH) and the best acceptor (basic nitrogen) groups in the theophylline molecule), which together with two bifurcated C \cdots O hydrogen bonds form chains.⁶⁸ (The lack of chains in the crystal structure of form IV is the characteristic feature

which distinguishes it from enantiotropically related form II⁸²) The character of the ^1H \cdots ^{14}N NQR spectra of theophylline recorded at 213 K (no indication of multiplets, Figure 2) confirms the presence of form II in the studied sample. Comparison of the deformation density maps, and NQR parameters obtained under the assumption of monomer and solid, Figure 3, Table 3, suggests that the intermolecular interactions in theophylline are much stronger than those in caffeine and less directional. The Hirshfeld surface with the normalized contact distance d_{norm} curvedness and shape index mapped over this surface for the whole theophylline and the vicinities of each nitrogen are shown in Figures 8 and 9. Because theophylline contains one methyl group less than caffeine, the Hirshfeld volume and surface are smaller, and, correspondingly, globularity and asphericity are larger than those observed for caffeine, Table 4. Results of the analysis of 2D fingerprint plot, summarized in Table 4, indicate stronger hydrogen bonds than those in caffeine. The red areas in the Hirshfeld surface describing N \cdots H \cdots N and C \cdots H \cdots O interactions are more clearly marked, Figure 4a. The characteristic wings, in the 2D molecular fingerprint d_e/d_i plot, Figure 8 are longer and well-separated and indicate the dominating directional interaction in the structure: N \cdots H \cdots N. The sharp wings at the top left, $d_i < d_e$, can be assigned to the surface around the donor (N \cdots H bond), whereas those at the bottom right, $d_e > d_i$, correspond to the surface around the acceptor (N). The area corresponding to the O \cdots H/H \cdots O and N \cdots H/H \cdots N contacts takes 12.6 and 27.2% of the total Hirshfeld surface, respectively, Figure 8, Table 4. The central part of 2D fingerprint plot for theophylline, Figure 8, reveals the presence of many H \cdots H interactions (protons from methyl groups), which takes 39% of the total Hirshfeld surface. These interactions are manifested as one common, highly broadened spike indicating the presence of several slightly different H \cdots H interactions. The curvedness and shape index are shown in Figure 5b and c. The adjacent red and blue triangles indicate that the crystal structure of theophylline exhibits $\pi\cdots\pi$ stacking interactions of 3.439 \AA and -57.4 kJ/mol i.e. much weaker than those in caffeine and competitive to N \cdots H \cdots N hydrogen bonds of 2.829 \AA and -39.2 kJ/mol . The analysis of the local Hirshfeld for each nitrogen site separately, reveals additional details, Figure 9. Two-dimensional fingerprints for N(7) and N(9) differ qualitatively and quantitatively from those for N(1) and N(3), Figure 9c-f and Table 5. Two sharp wings for N(7) and N(9) at the top are assigned to the surface around the (N \cdots C bonds), while the bottom corresponds to the surface around the (N \cdots H), unlike that for N(1) and N(3)—assigned to the surface around the (N \cdots C bonds), indicates different symmetry of the nitrogen vicinity, Figure 9. The subtle differences between methyl groups are not revealed by Hirshfeld, but they are visible on the deformation density map, Figure 4 and in experiment, Table 1.

Theobromine. Theobromine crystallizes in the $P21/c$ system with $a = 9.2990$, $b = 18.6980$, $c = 9.0381 \text{ \AA}$,⁶⁹ with $Z = 8$ and according to DSC and IR studies shows no polymorphism. Two molecules in the asymmetric unit form a pseudocentrosymmetric dimer linked by two strong NH \cdots O hydrogen bonds, which is a synthon for a layered structure of two-dimensional hydrogen-bonded network built of weak CH \cdots N and CH \cdots O hydrogen bonds.⁶⁹ The character of the ^1H \cdots ^{14}N NQR spectra of theobromine recorded at 295 K is in good agreement with the X-ray data. There is an indication of a multiplet in the NQR spectrum, but the resolution permitted

Table 4. Comparison of Total Hirshfeld Surface, Volume, Globularity, Asphericity, and Areas Corresponding to the Particular Contacts (Percent of the Hirshfeld Surface), Characterizing Caffeine, Theophylline, and Theobromine

compound	inequivalent molecule	N···O N···N [%]	O···H [%]	N···H [%]	H···H [%]	O···all [%]	N···all [%]	surface [\AA^2]	volume [\AA^3]	globularity [-]	asphericity [-]	
caffeine	five inequivalent molecules	K1	1.1	24	12.4	45.5	11.0	11.9	221.61	220.99	0.798	0.121
		K2	2.1	23.5	8.6	46.8	15.7	7.7	217.03	215.16	0.800	0.114
		K3	0.3	26.6	10.6	45.5	13.7	10.8	219.75	220.28	0.803	0.116
		K4	1.5	20.9	9.0	49.2	15.3	10.9	217.68	212.12	0.790	0.121
		K5	2.1	23.4	9.6	47.5	12.8	9.2	220.54	219.25	0.797	0.124
	averaged	K1–5	1.4	24.5	10.4	45.2	13.4	9.9	219.32	217.56	0.798	0.119
theophylline	TP1	2.0	27.2	12.6	39	17	12	200.14	195.52	0.814	0.106	
theobromine	two inequivalent molecules	TB1	3.9	27.0	12.1	37.2	17.7	11.9	195.46	192.98	0.826	0.139
		TB2	3.0	26.5	14.8	34.3	17.9	12.2	194.44	190.50	0.823	0.133
	averaged	TB1–2	3.8	22.2	14.3	37.5	14.6	11.0	194.95	191.74	0.8245	0.136

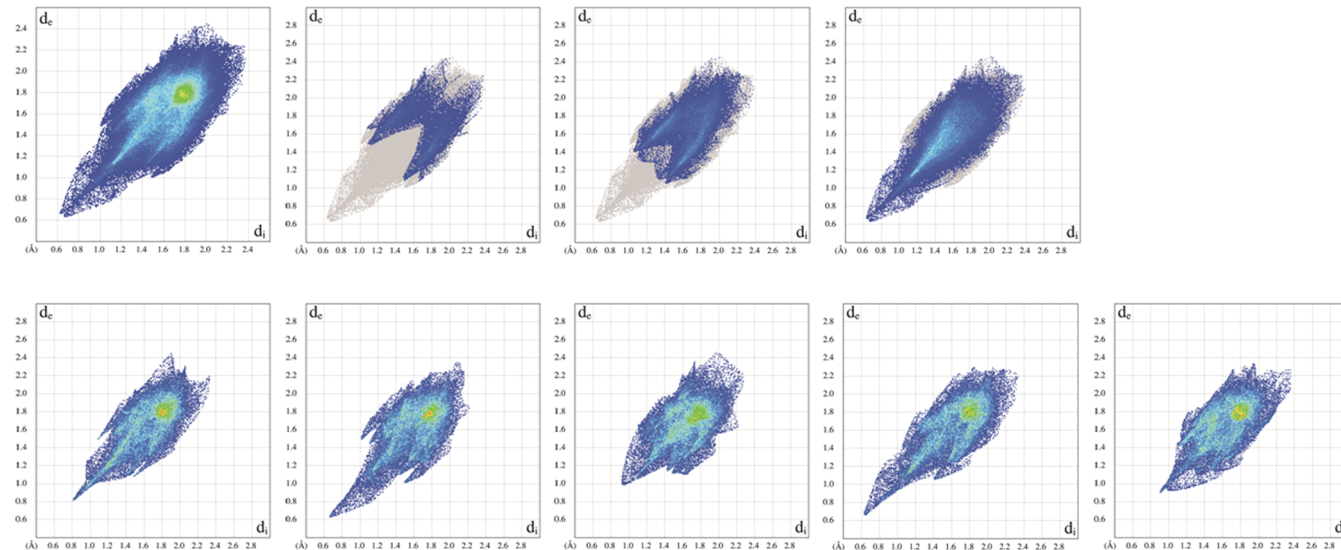


Figure 6. 2D molecular fingerprint d_e/d_i plot for caffeine (form β): (top) averaged over the crystal (total and separated NH, OH, and HH contributions) and (bottom) separated into five inequivalent molecules in the crystal (K1, K2, K3, K4, and K5).

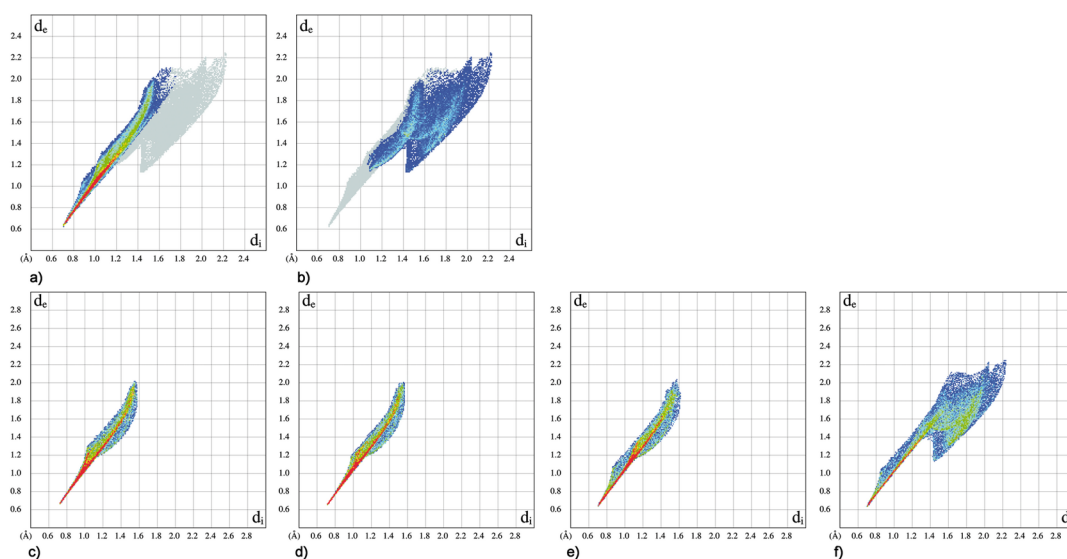


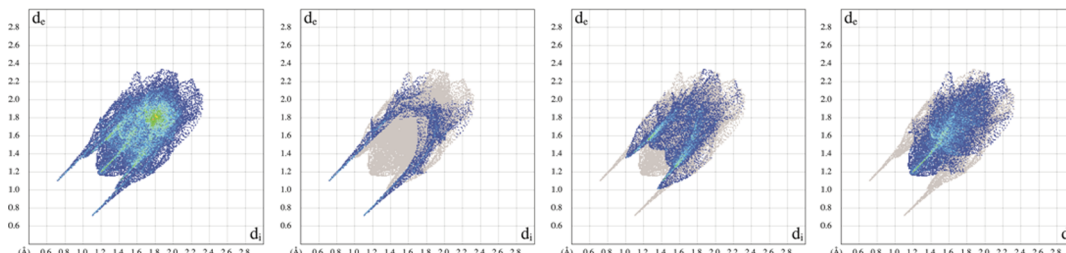
Figure 7. 2D molecular fingerprint d_e/d_i plot for nitrogen atoms in caffeine (form β): (a) NC (b) NH, (c) N(1), (d) N(3), (e) N(7), and (f) N(9).

only a separation of the lines assigned to $-\text{N}(9)=$ site. In general, the differences between the NQR parameters for both inequivalent molecules of theobromine are much larger than

between those obtained for caffeine, Table 1, but still small. The Hirshfeld surface with the normalized contact distance d_{norm} , curvedness and shape index mapped over this surface for

Table 5. Comparison of Total Hirshfeld Surface, Volume, Globularity, Asphericity, and Areas Corresponding to the N–C and N–H Bonds (Percent of the Hirshfeld Atomic Surface) for Caffeine, Theophylline, and Theobromine

compound	inequivalent molecule	site	N–C [%]	N–H [%]	surface [Å ²]	volume [Å ³]	globularity [-]	asphericity [-]
caffeine (five inequivalent molecules)	K1	N(1)	86.9	13.1	16.40	5.35	0.902	0.140
	K2	N(1)	86.3	12.2	16.34	5.33	0.903	0.135
	K3	N(1)	86.9	11.6	16.23	5.29	0.904	0.127
	K4	N(1)	87.3	12.7	16.35	5.33	0.903	0.139
	K5	N(1)	87.4	12.6	16.37	5.34	0.902	0.151
	K1	N(3)	86.8	13.2	16.10	5.19	0.900	0.139
	K2	N(3)	87.0	13.0	15.98	5.15	0.902	0.125
	K3	N(3)	85.9	14.0	16.01	5.16	0.902	0.130
	K4	N(3)	86.7	13.3	16.20	5.22	0.899	0.143
	K5	N(3)	86.6	13.4	16.20	5.22	0.899	0.148
	K1	N(7)	83.7	15.7	16.39	5.28	0.895	0.149
	K2	N(7)	82.1	17.9	16.17	5.20	0.898	0.129
	K3	N(7)	84.6	15.4	16.02	5.15	0.900	0.120
	K4	N(7)	82.7	15.8	16.48	5.31	0.893	0.149
	K5	N(7)	84.6	15.4	16.17	5.21	0.898	0.142
	K1	N(9)	41.1	58.6	24.44	10.41	0.944	0.024
	K2	N(9)	41.6	58.2	24.93	10.86	0.951	0.042
	K3	N(9)	42.6	56.7	24.86	10.72	0.946	0.028
	K4	N(9)	41.5	58.6	25.06	10.81	0.944	0.021
	K5	N(9)	40.7	59.3	26.25	11.62	0.945	0.022
theophylline	TP1	N(1)	85.7	12.7	16.79	5.53	0.901	0.137
	TP1	N(3)	85.9	14.1	16.34	5.28	0.897	0.141
	TP1	N(7)	45.7	53.0	20.27	6.90	0.864	0.126
	TP1	N(9)	47.9	52.1	22.00	8.47	0.914	0.071
theobromine (two inequivalent molecules)	TB1	N(1)	50.9	47.1	19.07	6.42	0.876	0.140
	TB2	N(1)	51.6	46.9	19.28	6.48	0.872	0.139
	TB1	N(3)	83.0	16.3	16.79	5.45	0.892	0.148
	TB2	N(3)	83.8	15.0	16.68	5.41	0.893	0.145
	TB1	N(7)	81.5	16.0	16.44	5.32	0.896	0.136
	TB2	N(7)	83.1	15.4	16.73	5.41	0.891	0.146
	TB1	N(9)	45.0	54.4	23.06	9.47	0.939	0.043
	TB2	N(9)	48.3	51.3	23.22	9.57	0.939	0.045

**Figure 8.** 2D molecular fingerprint d_e/d_i plot for theophylline: averaged over the crystal (total and separated NH, OH, and HH contributions).

the vicinities of each nitrogen in both inequivalent molecules and the whole theobromine molecule are shown in Figure 10. Theobromine as an isomer of theophylline contains the same number of methyl groups, thus its volume, surface, globularity, and asphericity differ only slightly from those of theophylline, Table 4. The size of red areas in the Hirshfeld surface, Figure 5 and the analysis of 2D fingerprint plot, Table 5, indicate the presence of hydrogen bonds N–H···O, CH···N, and CH···O differing in strength. The wings, in the 2D molecular fingerprint d_e/d_i plot, Figure 10, are long and well-separated. The area corresponding to the O···H/H···O and N···H/H···N contacts takes of 26.5–27.0 and 12.1–14.8% of the total Hirshfeld surface, respectively, Figure 10, Table 4. The central part of 2D fingerprint plot for theobromine similarly to theophylline and

caffeine, reveals the presence of many H···H contacts, Figure 10. These interactions are manifested as one common, strongly broadened spike but much smaller than those obtained for theophylline or caffeine as it takes only 34.3–37.2% of the total Hirshfeld surface. The curvedness and shape index are shown in Figure 5b and c. The adjacent red and blue triangles indicate that the crystal structure of theobromine exhibits $\pi\cdots\pi$ stacking interactions of 3.233–3.286 Å and of strength from –39.4 to –44.4 kJ/mol i.e. weaker than those in theophylline or caffeine and much weaker than two N–H···O hydrogen bonds of 2.850 Å and –36.5 kJ/mol linking molecules in dimers. Analysis of the local Hirshfeld for each nitrogen site performed similarly to those described earlier for caffeine and theophylline, reveals additional details. 2D Fingerprints for N(1) and N(9) differ

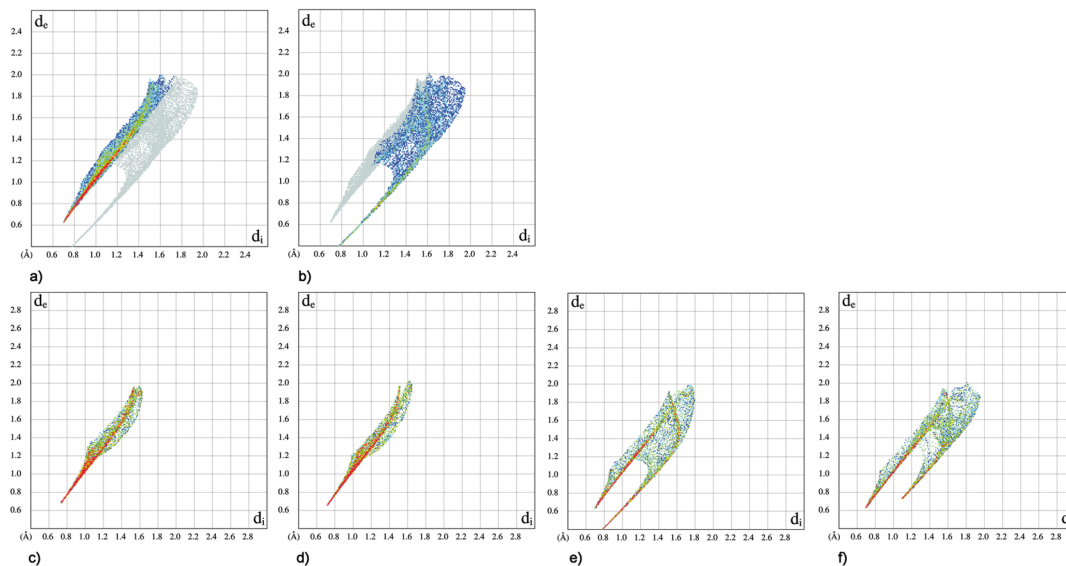


Figure 9. 2D molecular fingerprint d_e/d_i plot for nitrogen atoms in theophylline: (a) NC (b) NH, (c) N(1), (d) N(3), (e) N(7), and (f) N(9).

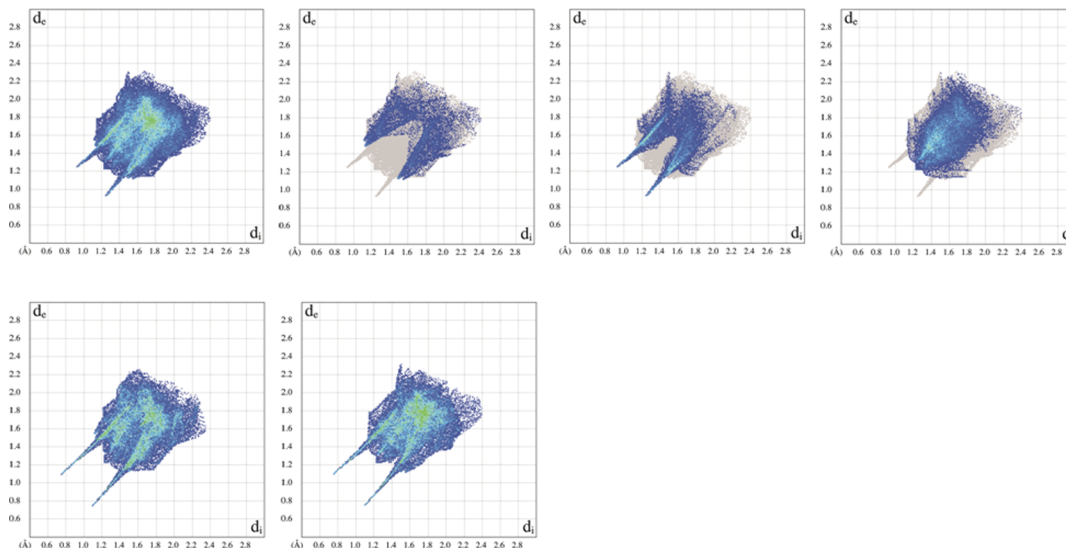


Figure 10. 2D molecular fingerprint d_e/d_i plot for theobromine. Averaged over the crystal: (top) total and separated NH, OH, and HH contributions and (bottom) separated into two inequivalent molecules in crystal (TB1 and TB2).

significantly from those for N(3) and N(7), Figure 11a–f and Table 5. Two wings for N(1) are long and sharp, the one at the top can be assigned to the surface around the (N—C bonds), while the one small and wide at the bottom corresponds to the surface around the (—NH), which is an acceptor in the N—H···O bond, Figure 11c. The two wings for N(9) differ from each other, the one at the top is long and sharp typical of N—C bonds, while the second at the bottom is small and wide and corresponds to the surface around the (—N=), which is an acceptor in the C—H···N bond, Figure 11f. The only one wide wing for N(3) and N(7) shows N—C bonds, Figure 11a, d, and e. The 2D fingerplot reveals differences in the symmetries of the nitrogen atoms vicinities and participation of N(1) in a strong bond, while N(9) in a weak one. The subtle differences between methyl groups, clearly visible on the deformation density map, Figure 4c, and in experiment, Table 1, are omitted. Comparison of the shape of 2D fingerprint plot for each corresponding nitrogen site in both inequivalent

molecules reveals the largest differences at N(9), Table 5, which is in good agreement with experiment, Table 1.

CONCLUSIONS

The differences in NQR spectra reflect the influence of the environmental effect, that is the participation of nitrogen atoms in intermolecular interactions. The discrepancy between experiment and theory suggests that the broadening of NQR lines is also a dynamical effect. The introduction of methyl groups to xanthine restricts the ability of nitrogen atoms to participate in strong hydrogen bonds, which is well-reflected by NQR parameters. The η parameter, which can be treated as a measure of intermolecular interactions strength is the highest in caffeine at N(9), in theophylline at N(7), while in theobromine at N(1), thus it indicates the sites involved in the strongest hydrogen bonds. Comparative analysis of the deformation density maps, NQR parameters, HS, and 2D fingerprints derived from them suggests that the intermolecular interactions in three methylxanthines differ significantly.

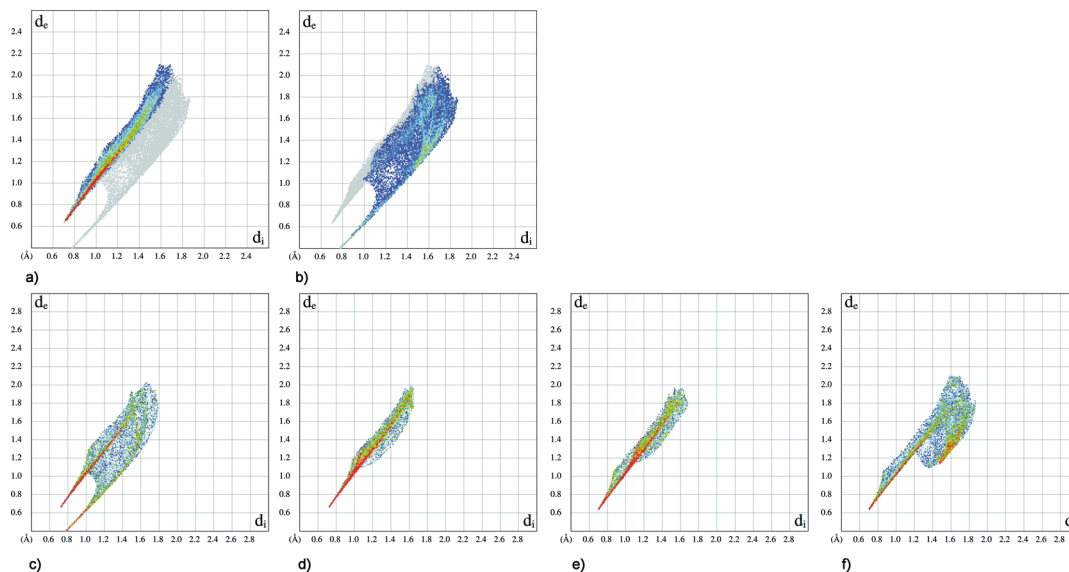
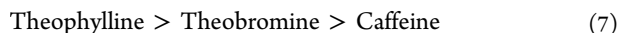


Figure 11. 2D molecular fingerprint d_e/d_i plot for nitrogen atoms in theobromine: (a) NC, (b) NH, (c) N(1), (d) N(3), (e) N(7), and (f) N(9).

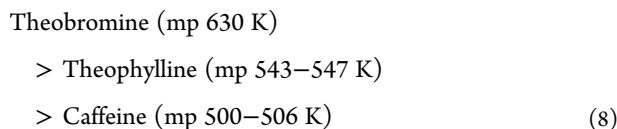
The dominating effect shifts from hydrogen bond (theophylline) to $\pi\cdots\pi$ stacking (caffeine). The weak $\pi\cdots\pi$ stacking in theobromine coincide with the flat tape ordering, while the strong $\pi\cdots\pi$ stacking in caffeine coincides with the disordered orientation of the planes containing the neighboring molecules. The orientation in theophylline is intermediate and suggests the equilibrium between both effect. The crystalline symmetry increases to orthorhombic when the interactions are in equilibrium and decreases when either of the two types of interactions dominates.

The ordering of methylxanthines according to decreasing strength of hydrogen bonds is



and it is in agreement with increasing quadrupole coupling constant at N(7) site. The ordering 7 is in a good agreement with the ordering according to increasing pK_a theophylline ($pK_a = 8.81$) < theobromine ($pK_a = 9.9$) < caffeine ($pK_a = 10.4$) and the ordering 2 i.e. according to cardiac stimulation, coronary dilatation, smooth muscle relaxation, diuretic, and goitrogenic potential.

It is slightly different than the ordering according to the increasing strength of $\pi\cdots\pi$ stacking



which is correlated with the ordering according to increasing both quadrupole coupling constant and asymmetry parameter at N(1).

The ordering 8 is in good agreement with that according to melting points (given in parentheses), which is often used as a crude measure of the strength of intermolecular forces. It is also correlated with the ordering according to water solubility at 25 °C, which is high for caffeine 21.600 g/L, lower for theophylline 7.360 g/L, and very low for theobromine 0.330 g/L and with the ordering 1 according to cardiac stimulation, coronary dilatation, smooth muscle relaxation, diuretic, and goitrogenic potential.

Thus, NQR parameters characterizing charge deformation and proton affinity at N(1) reflects the ordering 8 and 1, while those at N(7) reflect the ordering 7 and 2.

Recently, caffeine and theobromine have been found to be less potent inhibitors of adenosine deaminase (ADA) than theophylline, which acts as a noncompetitive inhibitor and has got two binding sites of ADA (inhibition constants: K_i 342 and 311 μM vs 201 and 56 μM , respectively). The quadrupole coupling constant at N(1) and N(7) sites is well-correlated with inhibition constant K_i , Figure 12, which highly supports

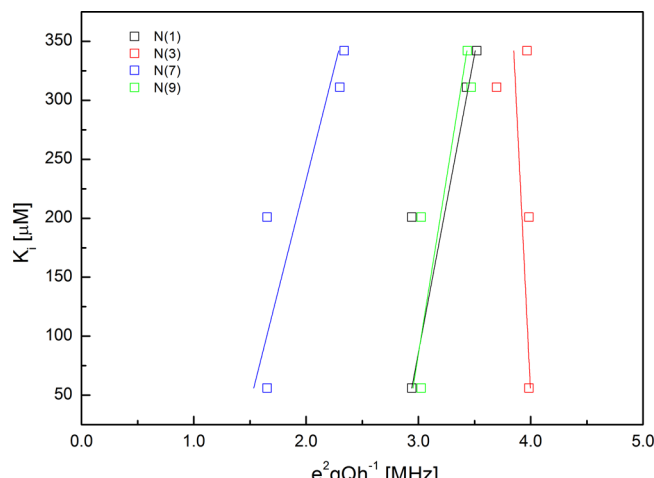


Figure 12. Correlation between inhibitor constant, K_i , and quadrupole coupling constant e^2Qq/h for all nitrogen atoms in methylxanthines (caffeine, theophylline and theobromine).

Moosavi-Movahedi et al.⁸⁶ and Ataie et al. hypothesis⁸⁷ concerning the role of N(1) and N(7) in binding affinity of the methylxanthine inhibitors to the enzyme.

AUTHOR INFORMATION

Corresponding Author

* E-mail: Jolanta.Latosinska@amu.edu.pl. Tel.: +48-61-8295277.

Notes

The authors declare no competing financial interest.

ACKNOWLEDGMENTS

The study was supported by the Foundation for Development Diagnostics and Therapy, Warsaw, Poland (J.N.L. and M.L.). Generous allotment of computer time from the Poznań Supercomputing and Networking Center (PCSS) in Poznań, Poland, is gratefully acknowledged (J.N.L. and M.L.).

REFERENCES

- (1) Suzuki, T.; Ashihara, H.; Waller, G. R. Purine and Purine Alkaloid Metabolism in Camellia and Coffea Plants. *Phytochemistry* **1992**, *31* (8), 2575–2584.
- (2) Alikaridis, F. Natural Constituents of Ilex Species. *J. Ethnopharmacol.* **1987**, *20* (2), 121–144.
- (3) Clifford, M. N.; Ramirez-Martinez, J. R. Phenols and Caffeine in Wet-Processed Coffee Beans and Coffee Pulp. *Food Chem.* **1991**, *40* (1), 35–42.
- (4) Mehr, C. B.; Biswal, R. N.; Collins, J. L.; Cochran, H. D. Supercritical Carbon Dioxide Extraction of caffeine from guaraná. *J. Supercrit. Fluids* **1996**, *9* (3), 185–191.
- (5) Li, S.; Hartland, S. A New Industrial Process for Extracting Cocoa Butter and Xanthines with Supercritical Carbon Dioxide. *J. Am. Oil Chem. Soc.* **1996**, *73* (4), 423–429.
- (6) Nathanson, J. Caffeine and Related Methylxanthines: Possible Naturally Occurring Pesticides. *Science* **1984**, *226* (4671), 184–187.
- (7) Hollingsworth, R. G.; Armstrong, J. W.; Campbell, E. Caffeine as a Repellent for Slugs and Snails. *Nature* **2002**, *417* (6892), 915–916.
- (8) Waller, G. R.; Macvean, C. D.; Suzuki, T. High Production of Caffeine and Related Enzyme Activities in Callus Cultures of Coffea Arabica L. *Plant Cell Rep.* **1983**, *2* (3), 109–112.
- (9) Wright, G. A.; Baker, D. D.; Palmer, M. J.; Stabler, D.; Mustard, J. A.; Power, E. F.; Borland, A. M.; Stevenson, P. C. Caffeine in Floral Nectar Enhances a Pollinator's Memory of Reward. *Science* **2013**, *339* (6124), 1202–1204.
- (10) Henkin, R. I.; Schultz, M.; Minnick-Poppe, L. Intranasal Theophylline Treatment of Hyposmia and Hypogesia: A Pilot Study. *Arch. Otolaryngol. Head Neck Surg.* **2012**, *138* (11), 1064–70.
- (11) Smith, B. D.; Gupta, U.; Gupta, B. S. *Caffeine and Activation Theory: Effects on Health and Behavior*; CRC Press: Boca Raton, 2007; p 382.
- (12) Grobbee, D. E.; Rimm, E. B.; Giovannucci, E.; Colditz, G.; Stampfer, M.; Willett, W. Coffee, Caffeine, and Cardiovascular Disease in Men. *N. Engl. J. Med.* **1990**, *323* (15), 1026–1032.
- (13) Jee, S. H.; He, J.; Whelton, P. K.; Suh, I.; Klag, M. J. The Effect of Chronic Coffee Drinking on Blood Pressure: A Meta-Analysis of Controlled Clinical Trials. *Hypertension* **1999**, *33* (2), 647–652.
- (14) Robertson, D.; Hollister, A. S.; Kincaid, D.; Workman, R.; Goldberg, M. R.; Tung, C. S.; Smith, B. Caffeine and Hypertension. *Am. J. Med.* **1984**, *77* (1), 54–60.
- (15) Nurminen, M.-L.; Niittynen, L.; Korpela, R.; Vapaatalo, H. Coffee, Caffeine and Blood Pressure: a Critical Review. *Eur. J. Clin. Nutr.* **1999**, *53* (11), 831–839.
- (16) Ross, G. W.; Abbott, R. D.; Petrovitch, H.; Morens, D. M.; Grandinetti, A.; Tung, K. H.; Tanner, C. M.; Masaki, K. H.; Blanchette, P. L.; Curb, J. D.; Popper, J. S.; White, L. R. Association of Coffee and Caffeine Intake with the Risk of Parkinson Disease. *J. Am. Med. Assoc.* **2000**, *283* (20), 2674–9.
- (17) Postuma, R. B.; Lang, A. E.; Munhoz, R. P.; Charland, K.; Pelletier, A.; Moscovich, M.; Filla, L.; Zanatta, D.; Rios Romenets, S.; Altman, R.; Chuang, R.; Shah, B. Caffeine for Treatment of Parkinson Disease: A Randomized Controlled Trial. *Neurology* **2012**, *79* (7), 651–658.
- (18) Popat, R. A.; Van Den Eeden, S. K.; Tanner, C. M.; Kamel, F.; Umbach, D. M.; Marder, K.; Mayeux, R.; Ritz, B.; Ross, G. W.; Petrovitch, H.; Topol, B.; McGuire, V.; Costello, S.; Manthripragada, A. D.; Southwick, A.; Myers, R. M.; Nelson, L. M. Coffee, ADORA2A, and CYP1A2: the Caffeine Connection in Parkinson's disease. *Eur. J. Neurol.* **2011**, *18* (5), 756–765.
- (19) Eskelinen, M. H.; Kivipelto, M. Caffeine as a Protective Factor in Dementia and Alzheimer's Disease. *J. Alzheimer's Dis.* **2010**, *20* (Suppl 1), S167–74.
- (20) Maia, L.; Mendonça, A. D. Does Caffeine Intake Protect from Alzheimer's disease? *Eur. J. Neurol.* **2002**, *9* (4), 377–382.
- (21) Biessels, G. J. Caffeine, Diabetes, Cognition, and Dementia. *J. Alzheimer's Dis.* **2010**, *20* (Suppl 1), S143–50.
- (22) Dórea, J. G.; da Costa, T. H. M. Is Coffee a Functional Food? *Br. J. Nutr.* **2005**, *93* (06), 773.
- (23) Smit, H. J. Theobromine and the Pharmacology of Cocoa. *Handb. Exp. Pharmacol.* **2011**, No. 200, 201–34.
- (24) Dubuis, E.; Wortley, M. A.; Grace, M. S.; Maher, S. A.; Adcock, J. J.; Birrell, M. A.; Belvisi, M. G. Theophylline Inhibits the Cough Reflex Through a Novel Mechanism of Action. *J. Allergy Clin. Immunol.* **2014**, *133* (6), 1588–98.
- (25) Orru, M.; Guitart, X.; Karcz-Kubicha, M.; Solinas, M.; Justinova, Z.; Barodia, S. K.; Zanoveli, J.; Cortes, A.; Lluis, C.; Casado, V.; Moeller, F. G.; Ferre, S. Psychostimulant Pharmacological Profile of Paraxanthine, the Main Metabolite of Caffeine in Humans. *Neuropharmacology* **2013**, *67*, 476–84.
- (26) Jones, P. A.; Gonzalgo, M. L. Altered DNA Methylation and Genome Instability: a New Pathway to Cancer? *Proc. Natl. Acad. Sci. U. S. A.* **1997**, *94* (6), 2103–2105.
- (27) Nkondjock, A. Coffee Consumption and the Risk of Cancer: An Overview. *Cancer Lett.* **2009**, *277* (2), 121–125.
- (28) Bøhn, S. K.; Blomhoff, R.; Paur, I. Coffee and Cancer Risk, Epidemiological Evidence, and Molecular Mechanisms. *Mol. Nutr. Food Res.* **2014**, *58* (5), 915–930.
- (29) Song, F.; Qureshi, A. A.; Han, J. Increased Caffeine Intake is Associated With Reduced Risk of Basal Cell Carcinoma of the Skin. *Cancer Res.* **2012**, *72* (13), 3282–3289.
- (30) Li, G.; Ma, D.; Zhang, Y.; Zheng, W.; Wang, P. Coffee Consumption and Risk of Colorectal Cancer: A Meta-Analysis of Observational Studies. *Public Health Nutr.* **2013**, *16* (2), 346–357.
- (31) Heffernan, T. P.; Kawasumi, M.; Blasina, A.; Andere, K.; Conney, A. H.; Nghiem, P. ATR-Chk1 Pathway Inhibition Promotes Apoptosis after UV Treatment in Primary Human Keratinocytes: Potential Basis for the UV Protective Effects of Caffeine. *J. Invest. Dermatol.* **2009**, *129* (7), 1805–1815.
- (32) Kerzendorfer, C.; O'Driscoll, M. UVB and Caffeine: Inhibiting the DNA Damage Response to Protect Against the Adverse Effects of UVB. *J. Invest. Dermatol.* **2009**, *129* (7), 1611–1613.
- (33) Lu, Y.-P.; Lou, Y.-R.; Xie, J.-G.; Peng, Q.-Y.; Liao, J.; Yang, C. S.; Huang, M.-T.; Conney, A. H. Topical Applications of Caffeine or (-)-epigallocatechin gallate (EGCG) Inhibit Carcinogenesis and Selectively Increase Apoptosis in UVB-induced Skin Tumors in Mice. *Proc. Natl. Acad. Sci. U. S. A.* **2002**, *99* (19), 12455–12460.
- (34) Sabisz, M.; Składanowski, A. Modulation of Cellular Response to Anticancer Treatment by Caffeine: Inhibition of Cell Cycle Checkpoints, DNA Repair and More. *Curr. Pharm. Biotechnol.* **2008**, *9* (4), 325–336.
- (35) Tarka, S. M., Jr; Applebaum, R. S.; Borzelleca, J. F. Evaluation of the Perinatal, Postnatal and Teratogenic Effects of Cocoa Powder and Theobromine in Sprague-Dawley/CD rats. *Food Chem. Toxicol.* **1986**, *24* (5), 375–382.
- (36) Tarka, S. M., Jr; Morrissey, R. B.; Apgar, J. L.; Hostetler, K. A.; Shively, C. A. Chronic Toxicity/Carcinogenicity Studies of Cocoa Powder in Rats. *Food Chem. Toxicol.* **1991**, *29* (1), 7–19.
- (37) Grice, H. C. Genotoxicity and Carcinogenicity Assessments of Caffeine and Theobromine. *Food Chem. Toxicol.* **1987**, *25* (10), 795.
- (38) Lee, H. J.; Lee, K. W.; Kang, K. S.; Kim, D. Y.; Park, H. H.; Lee, M. J.; Kim, H. S.; Kwon, I. B. Theobromine with an anti-carcinogenic activity, Lotte. Confectionery Co., Ltd. (Seoul, KR), US patent 6693104, 2004.
- (39) Latosińska, J. N.; Latosińska, M. Anticancer Drug Discovery - From Serendipity to Rational Design. In *Drug Discovery*; El-Shemy, H., Ed.; InTech: 2013; pp 35–74, Chapter 2.

- (40) Petzer, J. P.; Castagnoli, N.; Schwarzschild, M. A.; Chen, J.-F.; Van der Schyf, C. J. Dual-target-Directed Frugs that Block Monoamine Oxidase B and Adenosine A(2A) Receptors for Parkinson's Disease. *Neurotherapeutics JASEN* **2009**, *6* (1), 141–151.
- (41) Chen, J.-F.; Chern, Y. Impacts of Methylxanthines and Adenosine Receptors on Neurodegeneration: Human and Experimental Studies. *Methylxanthines; Handbook of experimental pharmacology*; Springer, 2011; Vol. 200, pp 267–310.
- (42) Mitchell, E. S.; Slettenaar, M.; vd Meer, N.; Transler, C.; Jans, L.; Quadt, F.; Berry, M. Differential Contributions of Theobromine and Caffeine on Mood, Psychomotor Performance and Blood Pressure. *Physiol. Behav.* **2011**, *104* (5), 816–822.
- (43) Ledwidge, M. T.; Corrigan, O. I. Effects of Surface Active Characteristics and Solid State Forms on the pH Solubility Profiles of Drug–Salt Systems. *Int. J. Pharm.* **1998**, *174* (1–2), 187–200.
- (44) Booyen, H. P.; Moraal, C.; Terre'Blanche, G.; Petzer, A.; Bergh, J. J.; Petzer, J. P. Thio- and Aminocaffeine Analogues as Inhibitors of Human Monoamine Oxidase. *Bioorg. Med. Chem.* **2011**, *19* (24), 7507–7518.
- (45) Latosińska, J. N.; Latosińska, M.; Seliger, J.; Žagar, V.; Maurin, J. K.; Kazimierczuk, Z. Nature of Isomerism of Solid Isothiourea Salts, Inhibitors of Nitric Oxide Synthases, as Studied by ^1H - ^{14}N Nuclear Quadrupole Double Resonance, X-Ray, and Density Functional Theory/Quantum Theory of Atoms in Molecules. *J. Phys. Chem. A* **2012**, *116* (S), 1445–1463.
- (46) Seliger, J.; Žagar, V.; Latosińska, M.; Latosińska, J. N. Electron Configuration and Hydrogen-Bonding Pattern in Several Thymine and Uracil Analogues Studied by ^1H - ^{14}N NQDR and DFT/QTAIM. *J. Phys. Chem. B* **2012**, *116* (30), 8793–8804.
- (47) Latosińska, J. N.; Latosińska, M.; Seliger, J.; Žagar, V.; Kazimierczuk, Z. Electron Density Distribution in Cladribine (2-chloro-2'-deoxyadenosine) – A Drug Against Leukemia and Multiple Sclerosis – Studied by Multinuclear NQR Spectroscopy and DFT Calculations. *Chem. Phys. Lett.* **2009**, *476* (4–6), 293–302.
- (48) Daly, J. W. Caffeine Analogs: Biomedical Impact. *Cell. Mol. Life Sci.* **2007**, *64* (16), 2153–2169.
- (49) Seliger, J.; Blinc, R.; Arend, H.; Kind, R. Proton- ^{14}N Double Resonance Study of the Structural Phase Transitions in the Perovskite Type Layer Compound $(\text{CH}_3\text{NH}_3)_2\text{CdCl}_4$. *Z. Phys. B: Condens. Matter* **1976**, *25* (2), 189–195.
- (50) Seliger, J.; Žagar, V. Measurement of the ^{14}N Nuclear Quadrupole Resonance Frequencies by the Solid Effect. *J. Magn. Reson.* **2008**, *193* (1), 54–62.
- (51) Seliger, J.; Žagar, V. New Methods for Detection of ^{14}N NQR Frequencies. *Appl. Magn. Reson.* **2012**, *43* (4), 469–484.
- (52) Blinc, R.; Mali, M.; Osredkar, R.; Prelesnik, A.; Seliger, J.; Zupančič, I.; Ehrenberg, L. ^{14}N NQR Spectroscopy of Some Amino Acids and Nucleic Bases via Double Resonance in the Laboratory Frame. *J. Chem. Phys.* **1972**, *57* (12), 5087–5093.
- (53) Seliger, J.; Žagar, V. Sensitivity of Nuclear-Quadrupole Double-Resonance Detection of Half-Integer Spin Nuclei. *J. Magn. Reson.* **2008**, *194* (2), 175–181.
- (54) Seliger, J.; Žagar, V.; Blinc, R. A New Highly Sensitive ^1H - ^{14}N Nuclear-Quadrupole Double-Resonance Technique. *J. Magn. Reson. A* **1994**, *106* (2), 214–222.
- (55) Seliger, J.; Žagar, V.; Blinc, R. ^1H - ^{14}N Nuclear Quadrupole Double Resonance with Multiple Frequency Sweeps. *Z. Naturforsch.* **1994**, *49a*, 31–34.
- (56) Frisch, M. J.; Trucks, G. W.; Schlegel, H. B.; Scuseria, G. E.; Robb, M. A.; Cheeseman, J. R.; Scalmani, G.; Barone, V.; Mennucci, B.; Petersson, G. A.; Nakatsuji, H.; Caricato, M.; Li, X.; Hratchian, H. P.; Izmaylov, A. F.; Bloino, J.; Zheng, G.; Sonnenberg, J. L.; Hada, M.; Ehara, M.; Toyota, K.; Fukuda, R.; Hasegawa, J.; Ishida, M.; Nakajima, T.; Honda, Y.; Kitao, O.; Nakai, H.; Vreven, T.; Montgomery, J. A., Jr.; Peralta, J. E.; Ogliaro, F.; Bearpark, M.; Heyd, J. J.; Brothers, E.; Kudin, K. N.; Staroverov, V. N.; Kobayashi, R.; Normand, J.; Raghavachari, K.; Rendell, A.; Burant, J. C.; Iyengar, S. S.; Tomasi, J.; Cossi, M.; Rega, N.; Millam, N. J.; Klene, M.; Knox, J. E.; Cross, J. B.; Bakken, V.; Adamo, C.; Jaramillo, J.; Gomperts, R.; Stratmann, R. E.; Yazayev, O.; Austin, A. J.; Cammi, R.; Pomelli, C.; Ochterski, J. W.; Martin, R. L.; Morokuma, K.; Zakrzewski, V. G.; Voth, G. A.; Salvador, P.; Dannenberg, J. J.; Dapprich, S.; Daniels, A. D.; Farkas, Ö.; Foresman, J. B.; Ortiz, J. V.; Ciosowski, J.; Fox, D. J. *Gaussian 09 Revision D.01*; Gaussian, Inc.: Wallingford CT, 2009.
- (57) Delley, B. An All-electron Numerical Method for Solving the Local Density Functional for Polyatomic Molecules. *J. Chem. Phys.* **1990**, *92* (1), 508–517.
- (58) Delley, B. From Molecules to Solids with the DMol³ Approach. *J. Chem. Phys.* **2000**, *113* (18), 7756–7764.
- (59) Becke, A. D. A New Mixing of Hartree–Fock and Local Density-Functional Theories. *J. Chem. Phys.* **1993**, *98* (2), 1372–1377.
- (60) Lee, C.; Yang, W.; Parr, R. G. Development of the Colle-Salvetti Correlation-Energy Formula Into a Functional of the Electron Density. *Phys. Rev. B* **1988**, *37* (2), 785–789.
- (61) Pyyykö, P. Year-2008 Nuclear Quadrupole Moments. *Mol. Phys.* **2008**, *106* (16–18), 1965–1974.
- (62) Spackman, M. A.; McKinnon, J. J. Fingerprinting intermolecular interactions in molecular crystalsBased on the presentation given at CrystEngComm Discussion, 29th June-1st July 2002, Bristol, UK. *CrystEngComm* **2002**, *4* (66), 378–392.
- (63) Spackman, M. A.; Jayatilaka, D. Hirshfeld Surface Analysis. *CrystEngComm* **2009**, *11* (1), 19–32.
- (64) Latosińska, J. N.; Latosińska, M.; Seliger, J.; Žagar, V.; Maurin, J. K.; Orzeszko, A.; Kazimierczuk, Z. Structural Study of Selected Polyhalogenated Benzimidazoles (Protein Kinase CK2 Inhibitors) by Nuclear Quadrupole Double Resonance, X-ray, and Density Functional Theory. *J. Phys. Chem. A* **2010**, *114* (1), 563–575.
- (65) Latosińska, J. N.; Latosińska, M.; Seliger, J.; Žagar, V.; Kazimierczuk, Z. An Insight Into Prototropic and Supramolecular Motifs in Solid-State Structure of Allopurinol, Hypoxanthine, Xanthine and Uric Acid. A ^1H - ^{14}N NQDR Spectroscopy and Hybrid DFT/QTAIM and Hirshfeld Surface-Based Study. *J. Phys. Chem. B* **2014**, DOI: 10.1021/jp504871y.
- (66) Latosińska, J. N. NQR parameters: Electric Field Gradient Tensor and Asymmetry Parameter Studied in Terms of Density Functional Theory. *Int. J. Quantum Chem.* **2003**, *91* (3), 284–296.
- (67) Lehmann, C. W.; Stowasser, F. The Crystal Structure of Anhydrous Beta-Caffeine as Determined from X-ray Powder-Diffraction Data. *Chemistry* **2007**, *13* (10), 2908–2911.
- (68) Ebisuzaki, Y.; Boyle, P. D.; Smith, J. A.; Methylxanthines, I. Anhydrous Theophylline. *Acta Crystallogr. Sect. C Cryst. Struct. Commun.* **1997**, *53* (6), 777–779.
- (69) Ford, K. A.; Ebisuzaki, Y.; Boyle, P. D. Methylxanthines. II. Anhydrous Theobromine. *Acta Crystallogr. Sect. C Cryst. Struct. Commun.* **1998**, *54* (12), 1980–1983.
- (70) Edwards, H. G. M.; Lawson, E.; Matas, M. d.; Shields, L.; York, P. Metamorphosis of Caffeine Hydrate and Anhydrous Caffeine. *J. Chem. Soc. Perkin Trans. 2* **1997**, No. 10, 1985–1990.
- (71) Matsuo, K.; Matsuoka, M. Kinetics of Solid State Polymorphic Transition of Caffeine. *J. Chem. Eng. Jpn.* **2007**, *40* (6), 468–472.
- (72) Derollez, P.; Correia, N. T.; Danède, F.; Capet, F.; Affouard, F.; Lefebvre, J.; Descamps, M. Ab initio Structure Determination of the High-temperature Phase of Anhydrous Caffeine by X-ray Powder Diffraction. *Acta Crystallogr. Sect. B, Struct. Sci.* **2005**, *61*, 329–334.
- (73) Enright, G. D.; Terskikh, V. V.; Brouwer, D. H.; Ripmeester, J. A. The Structure of Two Anhydrous Polymorphs of Caffeine from Single-Crystal Diffraction and Ultrahigh-Field Solid-State ^{13}C NMR Spectroscopy. *Cryst. Growth Des.* **2007**, *7* (8), 1406–1410.
- (74) Murugan, N. A.; Sayeed, A. Thermal Behavior of Disordered Phase of Caffeine Molecular Crystal: Insights from Monte Carlo Simulation Studies. *J. Chem. Phys.* **2009**, *130* (20), 204514.
- (75) Habgood, M. Form II Caffeine: A Case Study for Confirming and Predicting Disorder in Organic Crystals. *Cryst. Growth Des.* **2011**, *11* (8), 3600–3608.
- (76) Matsuo, K.; Matsuoka, M. Solid-State Polymorphic Transition of Theophylline Anhydrate and Humidity Effect. *Cryst. Growth Des.* **2007**, *7* (2), 411–415.

- (77) Kishi, Y.; Matsuoka, M. Surface Phenomena and Mechanism of Polymorphic Transition in Theophylline. *J. Chem. Eng. Jpn.* **2010**, *43* (3), 253–260.
- (78) Doser, H. Über die Schmelzpunkte des Pantokains, Bromurals und Theophyllins. *Archiv der Pharmazie* **1943**, *281* (7), 251–256.
- (79) Burger, A.; Ramberger, R. On the Polymorphism of Pharmaceuticals and Other Molecular Crystals. II. *Mikrochim. Acta* **1979**, *72* (3–4), 273–316.
- (80) Phadnis, N. V.; Suryanarayanan, R. Polymorphism in Anhydrous Theophylline—Implications on the Dissolution Rate of Theophylline Tablets. *J. Pharm. Sci.* **1997**, *86* (11), 1256–1263.
- (81) Suzuki, E.; Shimomura, K.; Sekiguchi, K. Thermochemical Study of Theophylline and its Hydrate. *Chem. Pharm. Bull.* **1989**, *37* (2), 493–497.
- (82) Khamar, D.; Pritchard, R. G.; Bradshaw, I. J.; Hutcheon, G. A.; Seton, L. Polymorphs of Anhydrous Theophylline: Stable Form IV Consists of Dimer Pairs and Metastable Form I Consists of Hydrogen-Bonded Chains. *Acta Crystallogr. Sect. C Cryst. Struct. Commun.* **2011**, *67* (12), o496–o499.
- (83) Seton, L.; Khamar, D.; Bradshaw, I. J.; Hutcheon, G. A. Solid State Forms of Theophylline: Presenting a New Anhydrous Polymorph. *Cryst. Growth Des.* **2010**, *10* (9), 3879–3886.
- (84) Khamar, D.; Pritchard, R. G.; Bradshaw, I. J.; Hutcheon, G. A.; Seton, L. Polymorphs of Anhydrous Theophylline: Stable Form IV Consists of Dimer Pairs and Metastable Form I Consists of Hydrogen-Bonded Chains. *Acta Crystallogr. Sect. C Cryst. Struct. Commun.* **2011**, *67*, o496–9.
- (85) (a) Naqvi, A. A.; Bhattacharyya, G. C. Crystal Data for Anhydrous Theophylline. *J. Appl. Crystallogr.* **1981**, *14* (6), 464. (b) Fucke, K.; McIntyre, G. J.; Wilkinson, C.; Henry, M.; Howard, J. A. K.; Steed, J. W. New Insights into an Old Molecule: Interaction Energies of Theophylline Crystal Forms. *Crys. Growth Des.* **2012**, *12* (3), 1395–1401.
- (86) Moosavi-Movahedi, A. A.; Safarian, S.; Hakimelahi, G. H.; Ataei, G.; Ajloo, D.; Panjehpour, S.; Riahi, S.; Mousavi, M. F.; Mardanyan, S.; Soltani, N.; Khalafi-Nezhad, A.; Sharghi, H.; Moghadamnia, H.; Saboury, A. A. QSAR Analysis for ADA Upon Interaction With a Series of Adenine Derivatives as Inhibitors. *Nucleos. Nucleot. Nucl.* **2004**, *23* (3), 613–624.
- (87) Ataiea, G.; Bagheria, S.; Divsalara, A.; Safarian, S.; Saboury, A. A.; Namaki, S.; Moosavi- Movahedi, A. A. A Kinetic Comparison on the Inhibition of Adenosine Deaminase by Purine Drugs. *Iran. J. Pharm. Res.* **2007**, *6* (1), 43–50.